

PATHOLOGICAL GAMMA OSCILLATIONS, IMPAIRED DOPAMINE RELEASE, SYNAPSE LOSS AND REDUCED DYNAMIC RANGE OF UNITARY GLUTAMATERGIC SYNAPTIC TRANSMISSION IN THE STRIATUM OF HYPOKINETIC Q175 HUNTINGTON MICE

T. ROTHE,^{a†} M. DELIANO,^{a†} A. M. WÓJTOWICZ,^{b†}
A. DVORZHAK,^b D. HARNACK,^d S. PAUL,^b T. VAGNER,^b
I. MELNICK,^{b,c} H. STARK^{a,†} AND R. GRANTYN^{b,d*}

^a Leibniz Institute for Neurobiology Magdeburg, Germany

^b Cluster of Excellence NeuroCure, Berlin, Germany

^c Bogomoletz Institute of Physiology, Kiev, Ukraine

^d Department of Experimental Neurology, University Medicine Charité, Berlin, Germany

Abstract—Huntington’s disease (HD) is a severe genetically inherited neurodegenerative disorder. Patients present with three principal phenotypes of motor symptoms: choreatic, hypokinetic-rigid and mixed. The Q175 mouse model of disease offers an opportunity to investigate the cellular basis of the hypokinetic-rigid form of HD. At the age of 1 year homozygote Q175 mice exhibited the following signs of hypokinesia: Reduced frequency of spontaneous movements on a precision balance at daytime (–55%), increased total time spent without movement in an open field (+42%), failures in the execution of unconditioned avoidance reactions (+32%), reduced ability for conditioned avoidance (–96%) and increased reaction times (+65%) in a shuttle box. Local field potential recordings revealed low-frequency gamma oscillations in the striatum as a characteristic feature of HD mice at rest. There was no significant loss of DARPP-32 immunolabeled striatal projection neurons (SPNs) although the level of DARPP-32 immunoreactivity was lower in HD. As a potential cause of hypokinesia, HD mice revealed a strong reduction in striatal KCl-induced dopamine release, accompanied by a decrease in the number of tyrosine hydroxylase-(TH)- and VMAT2-positive

synaptic varicosities. The presynaptic TH fluorescence level was also reduced. Patch-clamp experiments were performed in slices from 1-year-old mice to record unitary EPSCs (uEPSCs) of presumed cortical origin in the absence of G-protein-mediated modulation. In HD mice, the maximal amplitudes of uEPSCs amounted to 69% of the WT level which matches the loss of VGluT1+/SYP+ synaptic terminals in immunostained sections. These results identify impairment of cortico-striatal synaptic transmission and dopamine release as a potential basis of hypokinesia in HD. © 2015 IBRO. Published by Elsevier Ltd. All rights reserved.

Key words: Huntington’s disease, hypokinesia, gamma oscillations, corticostriatal, glutamate release, dopamine release.

INTRODUCTION

Huntington’s disease (HD) is a severe monogenetic disorder with a pathological gain of function. Disease progression is associated with a broad range of alterations in motor, cognitive and emotional performances eventually leading to dementia and premature death within an average of 20 years after the appearance of first symptoms (see (Walker, 2007; Ross et al., 2014) for a review of clinical studies). A characteristic feature of HD at earlier stages is the appearance of uncontrolled muscle contractions (chorea), whereas Parkinson-like symptoms, including hypokinesia, increased muscle tone and occasional tremor, are key symptoms of advanced HD. In 8–10% of cases (the Westphal variety of HD) the afflicted patients present without chorea and exhibit hypokinesia from the very beginning. The degree of motor impairment (hypokinesia, rigor and bradykinesia) but not chorea correlates with the neuropathological scores of disease severity (Rosenblatt et al., 2003).

Although the focus of the present report will be placed on the cellular basis of hypokinesia, it is deemed necessary to first provide a set of functional indicators of motor impairment to further characterize the selected mouse model of HD, the Z-Q175-KI mouse (Menalled et al., 2012). In comparison with the better known R6/2 HD mice, Q175 mice display motor disturbances at an older age and also survive longer, although the number of CAG repeats is extremely high (on average 184). At

*Correspondence to: R. Grantyn, Department of Experimental Neurology, University Medicine Charité, Robert-Koch-Platz 4, D-10115 Berlin, Germany.

E-mail address: rosemarie.grantyn@charite.de (R. Grantyn).

† These authors equally contributed to the material of this paper.

‡ With deep sadness we dedicate this publication to the memory of Holger Stark who suddenly died on the 18th of February, 2015.

Abbreviations: ACSF, artificial cerebrospinal fluid; dSPNs, SPNs of the direct pathway; EAs, evaluation areas; EGTA, ethylene glycol tetraacetic acid; HD, Huntington’s disease; HEPES, 4-(2-hydroxyethyl)-1-piperazineethanesulfonic acid; HOMs, homozygotes; iSPNs, SPNs of the indirect pathway; LFPs, local field potentials; mABs, monoclonal antibodies; MK-801, dizocilpine; NEM, N-ethylmaleimide; pABs, polyclonal antibodies; PBS, phosphate-buffered saline; PD, Parkinson’s disease; PPD, paired-pulse depression; PPF, paired-pulse facilitation; PPR, paired-pulse ratio; PSD, power spectral density; ROI, region of interest; SPNs, striatal projection neurons; TH, tyrosine hydroxylase; uEPSCs, unitary EPSCs; VFs, view fields; VGLUT1, vesicular glutamate transporter 1; WT, wild types.

the selected age of 1 year Q175 heterozygotes and homozygotes (HOMs) exhibit motor deficits for at least 4 months (Heikkinen et al., 2012; Menalled et al., 2012; Loh et al., 2013).

As for the cellular basis of the transition from chorea/hyperactivity to dystonia/hypokinesia we shall regard three principal possibilities: (i) sequential degeneration of neuronal subsets in the striatum, (ii) dopamine depletion and (iii) deficiency of corticostriatal synaptic transmission. Neuropathological studies of human HD brains suggested that the DRD2/enkephalin-expressing striatal projection neurons (SPNs) of the indirect pathway (iSPNs) undergo neurodegeneration before the DRD1/substance P-expressing SPNs of the direct pathway (dSPNs) decrease in number (Reiner et al., 1988; Sapp et al., 1995; Glass et al., 2000; Deng et al., 2004). According to the hypothesis of (Albin et al., 1989), the motor symptoms would then initially reflect the imbalance between the direct/indirect pathways with their facilitatory/suppressive role in motor activity and, later on, manifest the complete breakdown of signal transmission through the basal ganglia.

However, hypokinesia and rigidity might occur in the absence of substantial neuron loss in the striatum, as is the case in patients with the idiopathic parkinson syndrome (IPS) where motor impairments are mainly caused by the degeneration of dopaminergic neurons in the brain stem. Is then hypokinesia in HD caused by insufficiency of dopamine signaling (see (Cepeda et al., 2014) for a comprehensive review of clinical and animal studies)? Indeed, functional tests in HD preparations *in vitro* demonstrated reduced DA release (Petersen et al., 2002; Johnson et al., 2006; Callahan and Abercrombie, 2011; Dallerac et al., 2015) and impaired D1-dependent modulation of glutamatergic synaptic transmission (Joshi et al., 2009). It should be mentioned that some of these findings were stage-dependent, consistent with the notion that chorea might be associated with hyperactive dopamine signaling (Jahanshahi et al., 2010; Dallerac et al., 2015). Unfortunately, still little is known on the state of dopaminergic innervation and the capacity for striatal dopamine release of intact HD mice exhibiting hypokinesia. To fill this gap of knowledge was the second aim of the present study.

Finally, it had been suggested that corticostriatal uncoupling could be a cause of motor impairment in advanced HD (Cepeda et al., 2007; Joshi et al., 2009; Hong et al., 2012). However, the exact mechanism of lost corticostriatal control is still far from being understood. Since, for technical reasons, HD-related differences in the release characteristics of corticostriatal synapses are difficult to prove it has remained unclear whether reduced corticostriatal coupling is expressed at the level of individual corticostriatal connections or mainly due to degeneration of cortical pyramidal neurons. A first answer to this question could be obtained by recording unitary EPSCs (uEPSCs) of presumed corticostriatal origin. Such connections can be identified on the basis of their characteristic short-term plasticity, as it was shown that corticostriatal but not thalamostriatal EPSCs exhibit paired-pulse facilitation (PPF) under standard conditions (Ding et al.,

2008). The results of these experiments could then be confronted with the results of synapse counts using the vesicular glutamate transporter 1 (VGLUT1) as a marker of synaptic terminals of cortical origin (Deng et al., 2013).

On the whole, our material from 1-year-old Q175 mice renders support to the hypothesis that HD hypokinesia is associated with a reduction of dopaminergic and glutamatergic innervation in the striatum and occurs prior to the substantial loss of DARPP-32-labeled striatal projection cells.

EXPERIMENTAL PROCEDURES

Ethical approval

The present experiments were performed in fully adult mice from a colony of Z-Q175-KI provided by the CHDI (“Cure Huntington’s disease Initiative”) foundation. Every precaution was taken to minimize stress and to reduce the number of animals used in each series of experiments. The work described here has been carried out in accordance with the EU Directive 2010/63/EU for animal experiments and complies with the requirements for manuscripts submitted to biomedical journals. The work was registered at the Office of Health Protection and Technical Safety of the regional government Berlin (Landesamt für Arbeitsschutz, Gesundheitsschutz und Technische Sicherheit Berlin, T0448/12, G0006/13 and G0233/14).

Transgenic mice

The Z-Q175-KI mouse line was created by CHDI Fndn. Inc., Princeton, NJ, USA and provided by the Jackson Labs, Bar Harbor, USA (ME #370437). It originated from the Q140 knock-in (KI) mouse described by (Menalled et al., 2012) and expresses a chimeric mouse/human exon 1 *mhtt*. The mice were genotyped and analyzed for CAG length. The average CAG length was 184 ± 1.5 ($n = 19$). Experiments were either performed in Q175 wild types (WTs) or in HOMs. We shall refer to symptomatic mice carrying a mutant form of huntingtin as “HD mice” or just “HD”. All mice ranged within an age of 47–61 weeks (see Table 1 for means). Considering the absence of sex- and age-dependent differences in the tested parameters we have pooled the data from the WT and HD cohorts, unless mentioned otherwise.

Tests of motor activity

Circadian rhythm of spontaneous motor activity. Test cages identical to home cages were placed on the QS 4000 balance (Sartorius, Göttingen, Germany; resolution 0.1 g) situated in a sound-attenuating chamber. A white fluorescent lamp (8 W) served as a daytime light source and was turned on between 8 a.m. and 8 p.m. Animal movements were recorded every 2 s for 25 h and transferred to a personal computer using the software SartoConnect V3.1 (Sartorius, Göttingen, Germany) and a custom routine written in Visual Basic (courtesy of Dr. Horst Schicknick, LIN Magdeburg). Data was analyzed offline by taking the differences of adjacent weights as

Table 1. Summary of results

Parameter	WT		HD		<i>p</i> <	Test	% Difference	
	Mean, SE	<i>n</i>	Mean, SE	<i>n</i>			Meaning <i>n</i> *	
Age (d)	374.9 ± 6.0	21	367.0 ± 6.7	19	ns	MWU		Animals
Number CAG repeats			184 ± 1.5	19				Animals
Body weight (g)	32.5 ± 1.0	21	21.7 ± 0.8	19	0.0001	MWU	−33.3	Animals
Balance: Spont. movements in nonfamiliar environment (##/1st h)	1.0 ± 0.1	9	0.5 ± 0.04	7	0.01	ANOVA/Tukey	−55.0	Animals
Open field: Total distance run (m/10 min)	38.0 ± 2.1	10	27.5 ± 1.7	10	0.01	MWU	−27.6	Animals
Open field: Pause time (% total time spent)	13.8 ± 1.3	10	19.7 ± 1.5	10	0.01	MWU	+42.2	Animals
Shuttle box: Habituation (spont. compartment changes/30 min)	108.0 ± 6.8	5	45.3 ± 21.2	3	0.071	MWU	−58.0	Animals
Shuttle box – Session 3: Reaction times (s)	4.93 ± 0.09	300	8.17 ± 0.26	122	0.001	MWU	+65.7	Trials (5/3)*
Shuttle box – Session 3: Conditioned avoidance (% trials)	28.33 ± 0.01	300	1.11 ± 0.00	180	0.001	MWU	−96.1	Trials (5/3)*
Shuttle box – Session 3: Escape failures (% trials)	0.00 ± 0.00	300	32.22 ± 0.02	180	0.001	MWU	+32.2	Trials (5/3)*
LFPs in Str at quiet rest: Log rel. power at 37 Hz (“bipolar”)	−1.21 ± 0.06	5	−0.77 ± 0.17	3	0.071	MWU	+170	Animals
LFPs in Str at quiet rest: Log rel. power at 37 Hz (“monopolar”)	−0.69 ± 0.02	5	−0.25 ± 0.01	3	0.05	MWU	+170	Animals
LFPs: Av. corticostriatal coherence at 37 Hz	−0.20 ± 0.03	5	−0.36 ± 0.05	3	0.05	MWU	+80	Animals
Integral DA response to KCl 100 mM (% baseline)	39.14 ± 1.63 * 10 ³	4	4.79 ± 1.35 * 10 ³	4	0.05	MWU	−88	Animals
Striatal [DA] (nmol/mg protein)	0.84 ± 0.04	3	0.48 ± 0.02	3	0.01	MWU	−43	Animals
Number TH + /VMAT2+ varicosities/per EA 18 × 18	14.8 ± 0.33	120	13.2 ± 0.32	120	0.001	MWU	−10.8	EAs (2/2)*
Av. diameter TH + /VMAT2+ presynaptic areas (μm)	0.551 ± 0.005	65	0.519 ± 0.007	72	0.001	MWU	−5.8	ROIs (2/2)*
Av. presynaptic TH fluorescence intensity (a.u.)	585.4 ± 30.5	65	415.7 ± 27.3	66	0.001	MWU	−29.0	ROIs (2/2)*
Av. cytoplasmatic DARPP-32 fluorescence in a.u.	84.3 ± 3.4	105	53.5 ± 3.2	105	0.001	MWU	−36.5	Cells (2/2)*
Number DARPP-32 + somata/VF 100 × 100	15.75 ± 0.58	53	17.21 ± 0.67	48	0.1002	t		VFs (2/2)*
Number of VGLUT1 + /Syp+ terminals/VF 100 × 100	21.2 ± 0.73	155	16.76 ± 0.54	150	0.001	MWU	−30.9	EAs (3/3)*
Number of vGAT + /Syp+ terminals per soma perimeter	4.0 ± 0.2	140	3.2 ± 0.1	135	0.001	t	−20.0	EAs (3/3)*
<i>E/I</i> ratio synaptic varicosities	1.09 ± 0.16	3	0.87 ± 0.04	3				Animals
NEM: Max. amplitude unitary EPSCs in 120 trials (pA)	79.3 ± 8.7	10	54.5 ± 3.6	13	0.01	MWU	−31.3	Cells (7/7)*
NEM: Failure rate (%)	1.39 ± 0.71	8	3.43 ± 0.85	12	0.1260	MWU		Cells (7/7)*
Control: Max. amplitude unitary EPSCs in 120 trials (pA)	62.1 ± 5.3	11	39.7 ± 2.4	18	0.0001	t	−36.1	Cells (10/18)*
Control: Failure rate (%)	8.15 ± 2.46	11	17.42 ± 1.89	19	0.0189	MWU	+114	Cells (10/18)*

* Number of animals in brackets.

measure of motor behavior. To account for the genotype-dependent differences in body weight (Table 1), data from individual animals was normalized by subtracting the mean and dividing through the standard deviation across time. The number of movements determined in this way was averaged in 1-h bins.

Open field. The open-field test was used to assess both exploratory behavior and spontaneous locomotor activity. The mice were individually tested between 9 a.m. and 2 p.m. using an open-field box made of white plastic with 37 × 37-cm surface area and 19-cm-high walls, illuminated by a spot of 25 W placed 1 m above the shadow-free box. Monitoring of 10-min sessions was done by a video camera (Sony Handycam DCR-PC100E). The videos were digitized using Pinnacle Studio Plus, further processed using the free software VirtualDub 1.9.11, and finally analyzed using a custom routine written in Matlab (courtesy of Dr. Achim Engelhorn, LIN Magdeburg). The behavioral parameters registered were the total traveled distance in 10 min and the fraction of time spent pausing.

Shuttle-box conditioning. One of the more successful ways to condition mice to sensory stimuli is based on avoidance learning in a two-way shuttle-box system (H10-11M-XX-SF, Coulbourn Instruments, Allentown, PA, USA). Within a few days of training, mice learn to move from one compartment to the other upon presentation of light, i.e. a conditioned stimulus (CS). By their shuttle behavior, mice avoid the unpleasant effect of an electric foot shock via the grid floor (0.4-mA pulses for a maximum of 10 s) that serves as the unconditioned stimulus (UCS). Mice were for 30 min habituated without light and foot-shock signals. On the next day animals were subjected to two avoidance training sessions separated by a pause of 6 h, followed by a third training session on the next morning. The training sessions consisted of 60 trials with 30-s inter-trial intervals from trial onset to trial onset. Each trial was started by turning on the light of the compartment where the animal actually stayed. The light lasted maximally 15 s. The electric foot shock followed 5 s after light onset. The time from light onset to start of motor activity was recorded as reaction time. Moving to the safety compartment within 5 s after light onset was regarded as conditioned response (avoidance) while changing compartments after foot shock onset was classified as unconditioned response (escape). If the animal did not change compartments during foot shock stimulation the response was classified as failure of escape.

Recording and evaluation of local field potentials (LFPs)

For chronic implantation of recording electrodes, animals were anesthetized with 50 mg/kg i.p. pentobarbital and mounted in a stereotaxic frame. Bipolar electrodes were custom-made of two twisted Teflon-insulated stainless steel wires (SS-3T/HH, Science Products, Hofheim, Germany) and stereotaxically implanted into the right motor cortex 1 (A–P 2.0 mm, M–L 1.5 mm, D 1.3 mm)

and into the right dorsal striatum (A–P 0.5 mm, M–L 2.0 mm, D 2.7 mm). The coordinates are relative to the bregma. Two stainless steel skull screws were positioned caudally on the left and right sides (A–P 5.5 mm, M–L 2.5 mm) serving as reference and ground electrodes. The head mount with electrode contacts (Plastics One, Roanoke, VA, USA), and the stainless steel wires connecting the socket contacts and screws were fixed with dental cement on the skull. Animals were given a rest of 3 days before the recordings started.

All experiments were conducted during the light phase of the diurnal cycle. Animals were placed in an open-field arena located in a sound-attenuating and electrically shielded recording chamber. The leads were connected via a rotating swivel (custom-made, Leibniz Institute for Neurobiology) to an amplifier consisting of the head stage HS4 and the controller module DB4 (World Precision Instruments, Sarasota, FL, USA). Recorded potentials were amplified 5000×, low-pass filtered at 100 Hz, digitized by an A/D interface with a sampling rate of 500 Hz (MICRO 1401 *mkII*, Cambridge Electronic Design Ltd., Cambridge, UK) and stored on a disk of a personal computer.

Data was collected for 2 × 90 min at two consecutive days. Open-field behavior was videotaped using Pinnacle Studio Plus (Pinnacle Systems Inc., Mountain View, CA, USA), time-stamped, and synchronized with electrophysiological recordings. Videotapes were later reviewed and coded. Each behavioral episode was grouped into three categories for analysis: (1) quiet rest, (2) grooming and (3) exploration. Quiet rest was defined as the absence of overt movement. Grooming referred to stereotyped face washing. Exploration episodes consisted of extended phases of rearing and other locomotor activities (e.g. walking) for which distinct start and stop time points could be accurately defined through visual observation. Analysis was only conducted if behavior of a given category lasted ≥ 3.0 s.

The LFP recordings were analyzed offline using Spike2 (Cambridge Electronic Design Ltd., Cambridge, UK) software and custom routines written in Matlab (The MathWorks, Natick, MA, USA). Spectral analysis was carried out by applying a time-dependent Fourier transformation. The recordings were analyzed in 3-s time frames shifted through the recording period in 3-s time steps. After multiplication with a Hanning window and zero-padding, power spectral density (PSD) data for M1 cortical and striatal recording electrodes in each mouse were calculated from each time frame by a 4096 point Fast Fourier Transformation (FFT). To allow for level comparisons across different conditions and groups, the PSD was normalized and presented as a percentage of total spectral power. PSDs obtained for individual behavioral epochs were averaged across repeated engagements in the same behavior, yielding a PSD for each behavior in every mouse. This was done to minimize the effects of the heterogeneity of duration and frequency of the behavioral epochs on the frequency analysis. For time-evolving power spectra, recordings were analyzed in 1-s time frames shifted through the recording in 20-ms time steps using a script in Matlab.

Microdialysis for determination of KCl-induced dopamine release

Five days before the experiment, mice were prepared for stereotaxic implantation of a dialysis guide cannula (MAB 10.8.IC, Microbiotech, Stockholm, Sweden) into the right dorsal striatum (A–P 0.26 mm, M–L 2.0 mm *D* 2.0 mm). The animals were anesthetized with 50 mg/kg i.p. pentobarbital. The guide cannula was fixed on the skull with dental cement. All animals resumed normal behavior including feeding 3 h after surgery.

On the day of experiment, a microdialysis probe (MAB 10.8.2.Cu, SS, diameter 0.2 mm, window 2 mm, Microbiotech, Stockholm, Sweden) was inserted into the dorsal striatum via the implanted guide cannula and the dialysis probe was perfused with standard salt solution at the following concentration (in mM): NaCl 147 mM, KCl 3 mM, CaCl₂ 1.3 mM, MgCl₂ 1 mM. The flow rate was 0.74 µl/min. The probe was connected via a rotating swivel (custom made; Leibniz Institute for Neurobiology) to a pump (MAB20, Microbiotech, Stockholm, Sweden) and a microfraction collector (CMA140, CMA-Microdialysis, Stockholm, Sweden). 10-min samples were collected continuously. The dopamine release capacity was tested by a subsequent application of 50 mM and then 100 mM KCl. For further processing 6.3-µl dialyzate samples were transferred to a high-pressure liquid chromatography system (Agilent 1100, Agilent Technologies, Waldbronn, Germany). We used a microautosampler (Famos, LC Packings, Amsterdam, The Netherlands), a reversed-phased-column (YMC 50 * 1 mm, 3 µm, YMC Europe GmbH, Schermbek, Germany), an electrochemical detector (Intro, Antec Leyden, The Netherlands) with a flow cell VT-03 micro and an ISAAC reference electrode (potential 450 mV). The temperature was kept at 32.5 °C. The mobile phase consisted of NaH₂PO₄ (0.15 M), 1-octane sulfonic acid (2.45 mM), ethylenediaminetetraacetic acid (1 mM), sodium chloride (2 mM), pH 4.6, and 9% methanol. The basal value for dopamine in the dialyzates amounted to 0.66 ± 0.08 fMol/sample. This corresponds to 0.105 ± 0.13 fMol/µl. The reliable detection limit was 0.016 fMol/µl. The microdialysis data were converted into percentages of the “baseline level” consisting of the mean concentration value from 8 control samples obtained prior to each KCl application.

Tissue dopamine concentration

The procedure was described in (Sagala et al., 2012). Briefly, three animals per phenotype were sacrificed at the age of 12 months. Brains were removed, shock-frozen in nitrogen-cooled methylbutane. Cryostat sections were obtained and bilateral punches were taken from the dorsal striatum using a stainless steel cannula with an internal diameter of 1.15 mm. The tissue samples were homogenized and the concentration of dopamine was determined with HPLC.

Antibodies and dyes

The primary polyclonal antibodies (pAbs) recognized the vesicular glutamate transporter 1, VGLUT1 (Synaptic-

Systems, Goettingen, Germany, #135304), synaptophysin, SYP (Abcam, Cambridge, UK, #ab72242), vesicular monoamine transporter type 2, VMAT2 (Phoenix Europe GmbH, Karlsruhe, Germany, #H-V008) and tyrosine hydroxylase, TH (Merck Millipore, Darmstadt, Germany, #AB1542). The primary monoclonal antibodies (mAbs) recognized dopamine, dopamine- and cAMP-regulated phosphoprotein, M(r) 32 kDa, DARPP-32 (R&D Systems, Wiesbaden, Germany, #MAB4230) or microtubule associated protein 2, MAP2 (Sigma Aldrich, Munich, Germany, #M1406). For double- and triple-labeling experiments, mAbs and pAbs were combined. Our immunostaining protocol for TH and VMAT2 was adapted to the methods described by [Weihe et al. \(2006\)](#). Secondary antibodies were coupled to Alexa Fluor 488, 555 and 647 purchased from Invitrogen (Darmstadt, Germany). The intracellular tracer Alexa Fluor 568 was from Life Technologies GmbH, Darmstadt, Germany.

Immunocytochemistry

For subsequent immunostaining mice were deeply anesthetized with isoflurane and transcardially perfused with ice-cold phosphate-buffered saline (PBS) containing in mM: NaCl 138; KCl 2.7, Na₂HPO₄·7H₂O 10, KH₂PO₄ 2, pH 7.4, followed by a solution of 4% (w/v) paraformaldehyde in PBS, pH 7.4. The hemispheres were separated, for cryoprotection submerged into graded sucrose solutions (10%, 20%, and 30%) and embedded in Tissue-Tek OCT (Sakura Finetek, Staufen, Germany). Sagittal plane sections (20 µm) were cut using a Jung CM 1800 cryomicrotome (Leica Biosystems, Nussloch, Germany), mounted on SuperFrost Plus microscope slides (Carl Roth, Karlsruhe, Germany) and processed for immunocytochemistry following the protocol of ([Henneberger et al., 2005](#)). Briefly, after three rinses in PBS, sections were washed in PBS containing 0.1% gelatin and kept overnight at 4 °C in a humid chamber for on slide reaction with the primary antibodies diluted in PBS/gelatin, supplemented with 0.12% Triton X-100. After washes in PBS/gelatin, the secondary antibodies were applied for 1 h at room temperature (23–25 °C). Coverslips were mounted on glass slides using Vectashield containing DAPI (Vector Laboratories, Cambridgeshire, UK).

Quantitative fluorescence microscopy and synapse counts

The different Alexa fluorochromes of the triple-stained samples were excited by appropriate lasers at 488, 568 and 633 nm. Images were acquired via a 40× oil immersion objective (electronic zoom: 1.6) connected to the Axio Observer Z1 LSM700 of Zeiss (Oberkochen, Germany) or via a 63× oil immersion objective connected to the SP5 confocal microscope (HCX PL APO) of Leica Microsystems (Wetzlar, Germany).

Two WT/HOM pairs were processed for counts of TH +/VMAT2+ synaptic terminals. Three sections per animal, four view fields (VFs) per section and five evaluation areas (EAs) per VF were analyzed making

up for 120 EAs per genotype. The VFs had a size of $100 \times 100 \mu\text{m}$ and were acquired from the dorsal striatum, starting at the rostro-ventral curvature of the L1.6-mm section (see (Paxinos and Franklin, 2003)). The EAs were circular with a diameter of $30 \mu\text{m}$. Counts of dopaminergic synaptic terminals were performed within the boundaries of each EA. The latter were placed on neuropil to avoid the influence of void areas occupied by neuron somata. For synapse identification and quantification of VMAT2 or TH fluorescence we used the software Nemo 1.423, as described by Henneberger et al. (2005). TH+ varicosities were tagged for count if (1) they exhibited co-localization with VMAT2 and (2) the size of the co-localizing VMAT2+ spot fell within a predefined range of values (average area of suprathreshold pixels between 0.3 and $0.7 \mu\text{m}^2$). This procedure required fluorescence analysis in a region of interest (ROI) that only contained one TH+/VMAT2+ varicosity (see Fig. 7C). The size of these ROIs was set to 30×30 pixels ($1.875 \times 1.875 \mu\text{m}$). Values of average VMAT2 fluorescence intensity (F_{Mean}) and its standard deviation (SD) were determined and a threshold was calculated by $F_{\text{Threshold}} = F_{\text{Mean}} + K \times \text{SD}$. The diameter of the presynaptic area (D) was calculated assuming a circular shape of the supra-threshold VMAT2+ area. The validity of the threshold algorithm was verified by varying the coefficient K from 1.0 to 4.5 prior to final analysis. This affected the numerical results but did not change the relationships between the values obtained from the two genotypes. The presented results are based on $K = 2.5$, as this value gave the best match between the suprathreshold VMAT2 area and the position of the TH area. $F_{\text{TH-presyn}}$ was then computed in a similar way, using VMAT2 fluorescence as a reference channel. The intensity values of Fig. 7E represent the average intensity of supra-threshold TH+ pixels.

The DARPP-32 fluorescence intensity and the number of DARPP-32-positive somata per viewfield were determined from matched sections, i.e. sections of brains that were perfused, stained and imaged together using standard exposure times. A total of 50 VFs of $100 \times 100 \mu\text{m}$ were obtained from three animals per genotype aged 56–58 weeks. Small rectangular ROIs ($2.45 \times 2.45 \mu\text{m}$) were placed on the somata of the five most intensely stained neurons of a VF, avoiding the nuclear region. These intensity values were taken from 8-bit Tiff images and expressed in arbitrary units (a.u.) without any correction or thresholding. For the counts of DARPP-32+ neurons we applied appropriate gamma scaling of the confocal display to optimize detection even in the weakly stained neurons of HD mice.

The counts of VGLUT1+ or VGAT+ synaptic terminals are based on three WT/HOM pairs at 56–58 weeks of age. In each animal at total of 12 VFs of $100 \times 100 \mu\text{m}$ were acquired from a standard area in the dorsal striatum. The procedure was similar to that described for evaluation of VMAT2+/TH+ terminals, with some minor differences. In each view field, five circular evaluation areas (EA, diameter $30 \mu\text{m}$) were defined and aligned to the center of a DARPP-32-positive soma. Synapse counts were performed within

the boundaries of each EA. Thus, synapse numbers were determined from a total of 50–60 EAs per animal. A VGLUT1+ or VGAT+ immunofluorescent terminal was included into the count and automatically transferred into an Excel data sheet if the following two additional criteria were met: (1) co-localization with SYP, (2) the presynaptic area occupied by the suprathreshold VGLUT1+ or VGAT+ pixels ranged from 0.3 to $0.7 \mu\text{m}^2$ when $F_{\text{Threshold}}$ was set to $F_{\text{Mean}} + 2 \text{SD}$.

Preparation of brain slices

The animals were deeply anesthetized by inhalation of a mixture of isoflurane and carbogen (95% O_2 and 5% CO_2) and transcardially perfused with 60 ml of ice-cold ($\sim 4^\circ\text{C}$) saline containing (in mM): choline chloride 110, KCl 3, NaH_2PO_4 1.25, NaHCO_3 25, glucose 10, CaCl_2 0.5, MgCl_2 7, MK-801 0.001 (pH 7.25, 305 mosmol/l). The perfusion solution was supplemented with glutathione $5 \mu\text{M}$, Na pyruvate $500 \mu\text{M}$ and ascorbic acid 2.8mM . The brain was removed quickly ($\sim 1 \text{min}$), separated into two hemispheres and transferred to ice-cold oxygenated saline of the same composition. Sagittal slices of $300\text{--}400 \mu\text{m}$ were prepared with a vibrating microtome (Integralslice 7550PSDS, Campden Instruments Ltd., Loughborough, UK) and then maintained for at least 1 h in artificial cerebrospinal fluid (ACSF) that contained (in mM): NaCl 125, KCl 3, NaH_2PO_4 1.25, NaHCO_3 25, CaCl_2 2, MgCl_2 1, glucose 10, MK-801 0.001, pyruvic acid 0.5, glutathione 0.005 and ascorbic acid 2.8 (pH 7.35, 303 mosmol/l).

Solutions and chemicals

During the patch-clamp experiments the slices were superfused with ACSF. MK-801 $1 \mu\text{M}$ and bicuculline methiodide (BMI, $25 \mu\text{M}$), both from Sigma–Aldrich Munich, Germany, were added to block NMDA- and GABA(A) receptor-mediated currents. The following pharmacological agents were applied during specific tests at the indicated concentrations: N-ethylmaleimide (NEM, $50 \mu\text{M}$) from Sigma–Aldrich and tetrodotoxin (TTX, $1 \mu\text{M}$) from Abcam, Cambridge, UK.

Patch-clamp recording

For electrophysiological tests, slices were submerged into a perfusion chamber with a constant flow of oxygenated ACSF. The flow rate was set to $1\text{--}2 \text{ml min}^{-1}$. Temperature during the recordings was maintained at $26\text{--}27^\circ\text{C}$. Preceding experiments at various maintenance temperature (range -30°C) showed that under the given conditions slices from animals > 1 year were best maintained at this temperature, the quality criterion being the level of neuronal membrane potentials at break-in, in addition to the appearance of the slices.

Pipette resistance was $3\text{--}6 \text{M Ohm}$ when filled with the following saline (in mM): potassium gluconate 100, KCl 50, NaCl 5, CaCl_2 0.5, EGTA 5, HEPES 25, MgATP 2, GTP 0.3.

Electrophysiological signals were acquired using an EPC-8 amplifier (List, Darmstadt, Germany), a 16-bit AD/DA board (ITC-16, HEKA Elektronik, Lambrecht, Germany) and the software TIDA 4.11 (HEKA Elektronik, Lambrecht, Germany). The signals were sampled at a rate of 10 kHz and filtered at 3 kHz. Liquid junction potentials were not corrected. In neurons, the holding potential was set to -70 mV which is close to the resting membrane potential recorded in HD mice immediately after break-in. Access resistance was monitored by applying pulses of -10 mV. Cell capacitance and access resistance values were obtained by fitting a mono-exponential function to the capacitance transients. Only recordings with a series resistance below 30 M Ohm were accepted (in typical cases series resistance amounted to 15–20 M Ohm). Series resistance compensation was not applied. Cells exhibiting more than a 20% change in the access resistance during an experiment were discarded.

The records were limited to the dorsal striatum. Striatal projection neurons (SPNs, equivalent to medium spiny neurons, MSNs, of morphological studies) were identified by their inward rectification and the long latency to the first spike (Kita et al., 1984; Nisenbaum and Wilson, 1995).

Electrical stimulation and recording of uEPSCs

Unitary evoked excitatory postsynaptic currents (uEPSCs) were elicited by intrastriatal microstimulation via a glass pipette filled with ACSF as described before (Dvorzhak et al., 2013b). Briefly, ACSF-filled glass pipettes with a resistance of 10 M Ohm were moved in the dorsal striatum in the vicinity of the recorded neuron until the recording pipette detected a postsynaptic response. Sometimes the recorded neurons were filled with Alexa 568 hydrazide which helped to avoid positions that could lead to direct depolarization of dendrites. An isolated stimulation unit was used to generate rectangular electrical pulses. Pulse duration was set to 0.5 ms. Pulse intensity was adjusted to activate a synaptic response at minimal intensity and with distinct threshold. Stimulation was accepted as unitary if the following criteria were satisfied: (1) uEPSC latency remained stable ($< 20\%$ fluctuations), (2) lowering stimulus intensity by 20% resulted in a complete failure of uEPSCs, (3) an increase in stimulus intensity by 20% neither changed mean uEPSC amplitude nor uEPSC shape, (4) there was no contamination by GABAergic synaptic input. On few occasions ($< 3\%$) paired-pulse trials produced failures in both the first and the second response. These trials were disregarded but the experiment continued if the regression slope of the amplitude plot against stimulus number remained zero. If double failures occurred more than 3 times in succession the experiment was discontinued. Typical current intensities required for unitary stimulation ranged from 0.4 to 0.6 μ A. Paired pulses were delivered at an inter-stimulus interval of 50 ms at a repetition frequency of 0.1–0.2 Hz to allow for full recovery of transmitter release after paired-pulse stimulation. Sites producing responses with a paired-pulse ratio (PPR) < 1 were discarded, as it was assumed that these inputs could be due to activation

of thalamic afferents. The search time required for finding a site giving rise to uEPSCs with a PPR ≥ 1 ranged from 10 to 45 min (average 32 min). For the sake of simplicity, uEPSCs with PPR will in the following text be referred to as EPSCs, assuming that in the vast majority of cases we have dealt with unitary connections of cortical origin.

Data evaluation and statistics

All data was evaluated off-line using TIDA 4.11 (HEKA Elektronik, Lambrecht, Germany), IgorPro6.0 (WaveMetrics, Lake Oswego, OR, USA), Prism 6.01 (Graphpad, San Diego, USA), SPSS 21 (SPSS GmbH Software, Munich, Germany).

The quantitative results are presented as mean \pm SEM. The error bars in the figures indicate SEM. Data points and means from HD mice are presented with gray fill. If not mentioned otherwise, the numbers in brackets are the number of tested neurons. Normality of data distributions was evaluated by the Kolmogorov–Smirnov or the Shapiro–Wilk test. Differences between means were determined by paired or unpaired *t*-test (normally distributed data) or Mann–Whitney *U*-test (not normally distributed data). Bonferroni correction was implemented in case of multiple comparison tests. A one-way ANOVA (normally distributed data) or Kruskal–Wallis statistics (not normally distributed data) was used for differences between three groups of data from different cells. Two-way ANOVA with post hoc Bonferroni correction was performed for experiments in the classical 2×2 design, with two independent factors (genotype and treatment). Time-course data were subjected to a repeated measures ANOVA followed by Tukey's multiple comparisons test. The asterisks in the figures indicate the following: * $p < 0.05$, ** $p < 0.01$, and *** $p < 0.001$.

RESULTS

Signs of hypokinesia in Q175 mice

When evaluating the motor activities in HD mice it is necessary to take into account the circadian rhythms of activity and sleep (Loh et al., 2013), as HD-related deviations might be more prominent at night. The graph of Fig. 1 presents the motor activity as the number of deflections registered by a sensitive Sartorius balance throughout an entire light–dark (LD) cycle in a sound-proof cage. During the night period HD mice displayed hyperactivity in the form of a delayed decline of the initial movement peak, consistent with a chorea-type disturbance. However, the first daytime confrontation with the settings of the recording system resulted in weaker exploratory activity in HD (about 50% of WT level) until both HD and WT resumed their characteristic daytime rest. The resulting overall light–dark pattern was more flat in HD.

The following tests were performed during the light phases, typically between 9 a.m. and 2 p.m. Fig. 2A, B presents the motor activity during an open-field test. Both indicators, i.e. the total distance covered (Fig. 2C) and the percent fraction of time spent in pauses (Fig. 2D), point to decreased spontaneous exploratory activity of HD mice during daytime. Similar results were

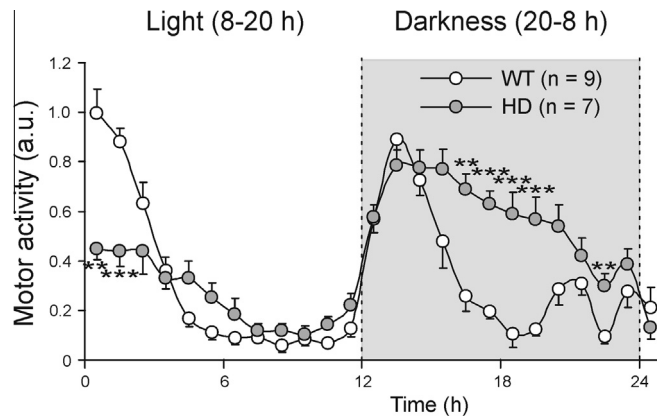


Fig. 1. HD-related differences in exploratory activity during the light period and motor behavior during darkness. ** $p < 0.01$, *** $p < .001$ using two-factor ANOVA, followed by Tukey's post hoc comparisons. a.u., arbitrary units; n , number of animals.

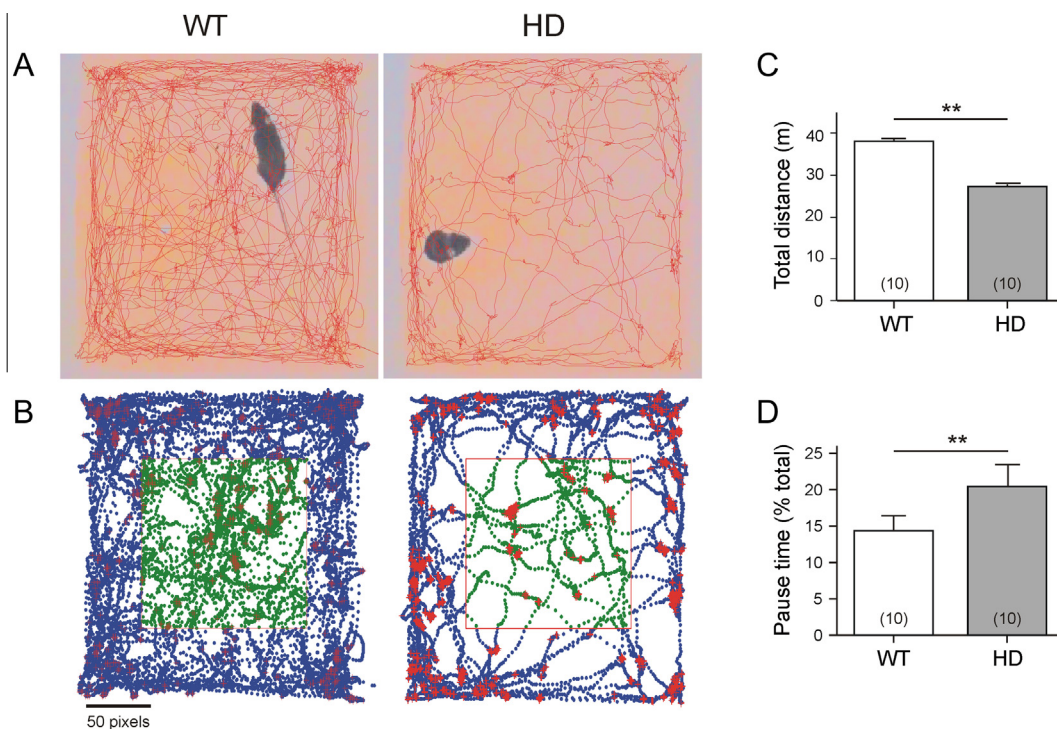


Fig. 2. Impaired locomotion in the open field test. (A) Locomotor trajectories within a period of 10 min. The WT mouse is walking, the HD mouse is sitting at the time of image acquisition. (B) Graphical presentation of motor activity outside (blue) and inside (green) of the central test area. Sites of pauses in red. (C) Total traveled distance in 10 min. (D) Fraction of time spent without movement. ** $p < .01$, Mann–Whitney U -test. In brackets: Number of animals. (For interpretation of the references to color in this figure legend, the reader is referred to the web version of this article.)

obtained when recording the motor activity of mice during habituation of exploratory activities in a shuttle box (Fig. 3A). In general, these findings are in line with the more comprehensive behavioral tests of (Menalled et al., 2012; Heikkinen et al., 2012).

In order to provide more specific information on the initiation of stimulus-induced motor responses we tested WT and HD mice in the classical 2-compartment shuttle box (Stark et al., 2004). These experiments revealed a significant prolongation of reaction times during performance of both unconditioned and conditioned motor

responses (Fig. 3B). Moreover, in a large number of trials HD mice failed to respond to electric shocks with an escape reaction (Fig. 3C). Finally, HD mice were unable to perform a conditioned response to light (Fig. 3D). Presented are the animal means from 60 trials. Table 1 presents the comparison of individual trials for session 3.

All these observations point to an HD-related deficit in movement initiation and will be pooled under the descriptive term “hypokinesia”, although different mechanisms might be addressed with each test or parameter. Among other possibilities one will have to

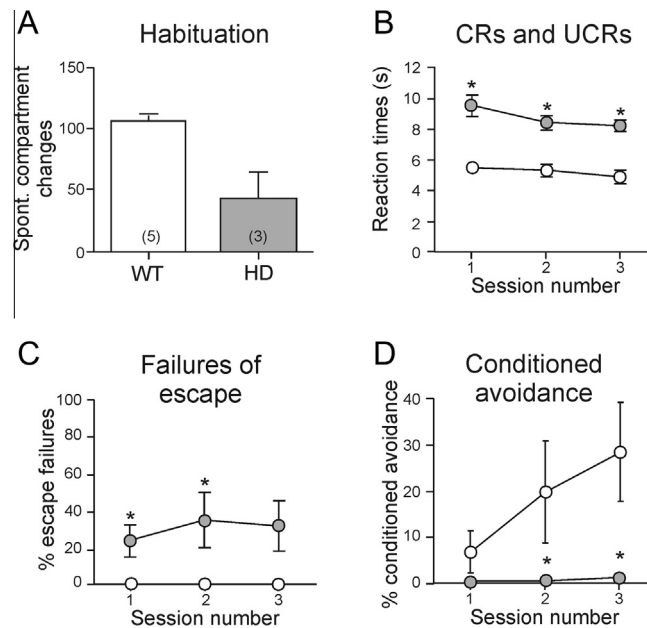


Fig. 3. Impaired shuttle-box behavior in HD. (A) Number of spontaneous compartment changes during a 30-min habituation period. (B) Reaction times in conditioned responses (CRs) and unconditioned responses (UCRs). (C) Percent fraction of unsuccessful escape responses to the electrical stimulus. (D) Percent fraction of conditioned avoidance responses. (D) White circle: WT, gray circle: Q175 HOM. * $p < .05$, Mann–Whitney U -test. Compared were the animal means, not the values obtained from individual trials. n , number of animals.

consider an increased threshold for the perception of noxious stimuli (Perrotta et al., 2012).

Pathological gamma oscillations in the striatum of hypokinetic HD mice at rest

An obvious question to ask is the following: If hypokinetic HD mice prevail in the resting state instead of utilizing sensory stimuli to execute appropriate movements, is their state of rest any different from that of WT mice? Simultaneous monopolar LFP recordings from the dorsal striatum and motor cortex of resting mice revealed that, indeed, the resting state of HD mice deviates from that of WT. In monopolar recordings HD but not WT exhibited characteristic gamma oscillations around 38 Hz in the striatum and, to lesser degree, in the motor cortex (Fig. 4). Grooming and exploratory behaviors were associated with the disappearance of the 38 Hz peak in the monopolar recordings from the HD striatum (not illustrated). To obtain some information on the origin of these oscillations we also analyzed bipolar LFP recordings (Fig. 5A). In this case gamma oscillations were much more prominent in the striatum, consistent with the hypothesis that the oscillatory activity is not passed on from the cortex but originates in the striatum itself. Again, grooming and exploratory activity were not associated with gamma oscillations (Fig. 5A, middle and right panel).

Analysis of phase and amplitude coupling between cortical and striatal activity was expected to provide further information, since a high degree of synchronicity is in general regarded as an indicator of effective signal transmission between two synaptically connected structures (von Nicolai et al., 2014). It is therefore interesting that coherence plotted as a function of frequency

exhibited a significant elevation in HD but not WT (Fig. 5B). However, this effect might merely reflect the enhanced power of deflections in the 33–42 range in the HD striatum. More work is obviously needed to clarify the origin of the pathological gamma oscillations at rest.

Impaired depolarization-induced dopamine release in HD

Numerous previous studies in the field of Parkinson's disease (PD) as well as other neurodegenerative conditions associate hypokinesia with insufficient supply of dopamine (see (Andre et al., 2010; Wichmann et al., 2011)). However, to the best of our knowledge, neither in Q175 mice nor in other mouse models of HD dopamine release has been estimated in intact mice.

To fill this gap of knowledge we tested a total of 4 WT and 4 Q175 HOMs for their capacity to release dopamine in response to KCl-induced depolarization. Under the given conditions maximal dopamine release was obtained with 100 mM KCl. The averaged traces of Fig. 6A illustrate the dramatic differences in the release capacity of WT and HD mice. The plots of Fig. 6B, C summarize the results obtained with KCl at a concentration of 50 and 100 mM, respectively. It can be seen that in HD mice the average dopamine response expressed as % change with respect to pre-KCl baseline level remained significantly under the response of WT mice (Fig. 6A, C). The absolute values of baseline dopamine release (in fMol/ μ l) were not different between the genotypes (data not shown), which might be due to the small number of animals tested, differences in the probe position and time after implantation.

As a step toward clarifying the HD-related difference in depolarization-induced dopamine release we also

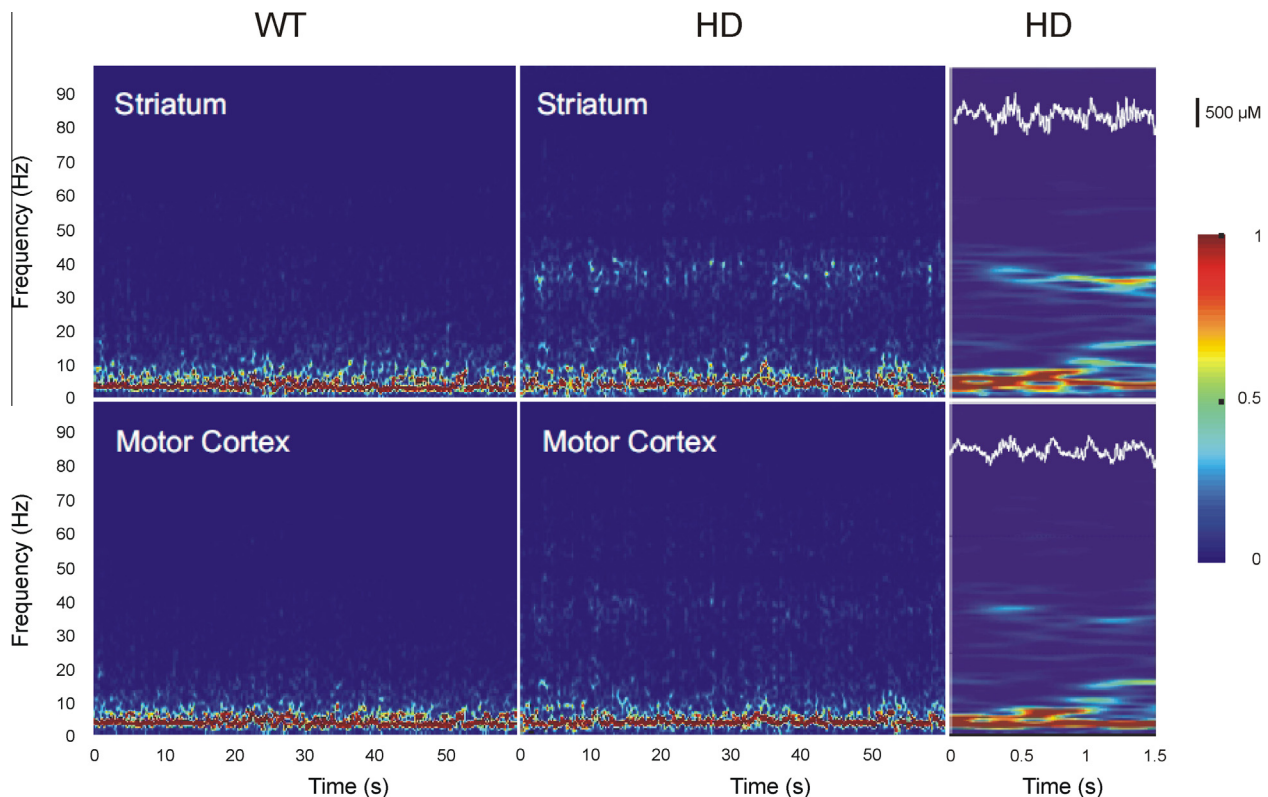


Fig. 4. Pathological oscillatory activities in the low gamma frequency range in the striatum and, to lesser extent, in the motor cortex of Q175 homozygotes. Color-coded power vs. frequency-time during behavioral states of rest. Right panel shows power plots and LFP traces at higher time resolution. (For interpretation of the references to colour in this figure legend, the reader is referred to the web version of this article.)

determined the dopamine concentration in frozen sections, following the procedure of Sagala et al. (2012). The results are presented in Fig. 6 and Table 1. We conclude that not only depolarization-induced dopamine release but also tissue dopamine levels at rest are severely compromised in the striatum of Q175 HD mice.

Reduced number of TH+/VMAT2+ axon terminals and lower level of presynaptic TH in HD mice

The pathophysiological mechanisms underlying the deficiency of DA release in hypokinetic HD mice are not yet clear. Previous studies reported an HD-related reduction of TH immunoreactivity in the murine (Ariano et al., 2002) and human (Bedard et al., 2011) striatum, which may reflect insufficient innervation by the ascending dopaminergic afferents from the *substantia nigra pars compacta* and/or lower levels of TH in the presynaptic elements. To further explore these possibilities, we performed an analysis of VMAT2 and TH co-localization in single axonal varicosities. Fig. 7A presents representative confocal images from WT and HD. Counts of VMAT2+ and TH+ varicosities in EAs of $16 \times 16 \mu\text{m}$ revealed an HD-related reduction in the number of TH+/VMAT2 synaptic terminals by 10.8% (Fig. 7B). The absolute numbers were 14.8 ± 0.33 in WT and 13.2 ± 0.32 in HD (Table 1). This finding is consistent with the hypothesis that, indeed, fewer synaptic terminals are available for dopamine release in the dorsal striatum.

To further clarify the possible cause of impaired DA release we evaluated single immunostained spots to characterize the presynaptic area made up by VMAT2 fluorescence in TH+ spots (Fig. 7C). The graph of Fig. 7D shows a reduced mean diameter of presynaptic VMAT2 fluorescence in TH+ varicosities. Furthermore, the average TH fluorescence estimated in VMAT2+ varicosities was significantly reduced in HD (Fig. 7E). Together, these results point to a presynaptic deficit in dopaminergic afferents.

Reduced immunoreactivity of DARPP-32 in HD mice

DARPP-32 immunoreactivity is enriched in SPNs (Anderson and Reiner, 1991) and plays a significant role in DR1-dependent functional enhancement of AMPARs, NMDARs, as well as voltage-activated Na and Ca channels (Bateup et al., 2010). The chronic lack of DARPP-32 affects motor activity according to the role of DR1- and DR2-expressing neurons in the basal ganglia circuitry. In HD mice, the levels of DARPP-32 message and protein fall below WT levels at early stages of the disease (Bibb et al., 2000).

Here we aimed at quantifying the DARPP-32 immunoreactivity of single SPNs at the age of 1 year, when HD mice exhibit symptoms of hypokinesia and reduced dopamine release. As expected, HD SPNs showed much weaker somatic fluorescence (Fig. 8A). For further quantification of DARPP-32 immunofluorescence ROIs of $2.45 \times 2.45 \mu\text{m}$ were placed on the

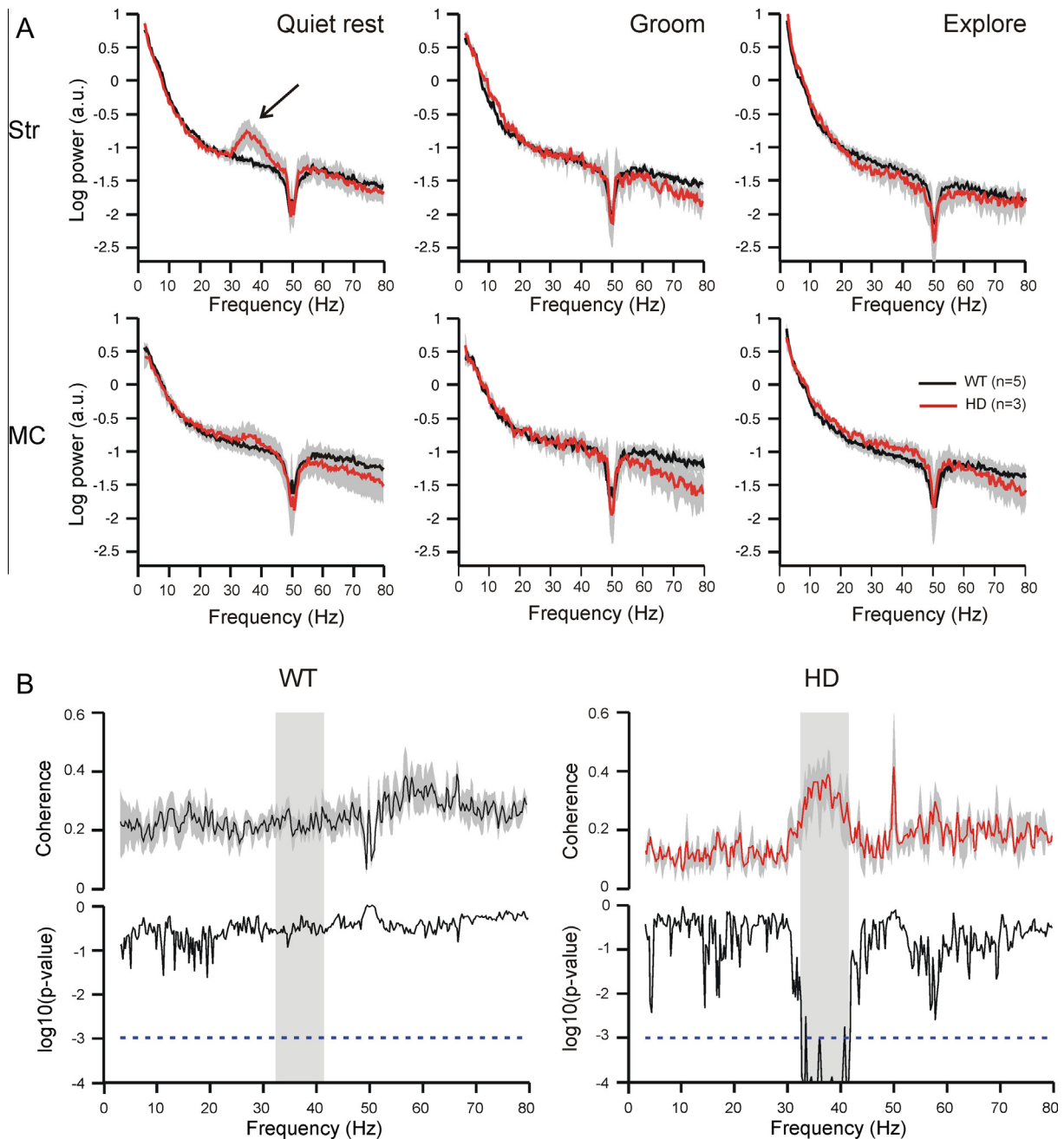


Fig. 5. Pathological oscillatory activities in the low gamma frequency range in the striatum (Str) and, to lesser extent, in the motor cortex (MC) of Q175 homozygotes. Evaluation of bipolar recordings. (A) Time-averaged power spectra during three different behavioral states. Solid lines represent the mean density, gray shades indicate SEM. The 50-Hz artifact due to power line noise has not been digitally suppressed. a.u., arbitrary units. Note HD-related elevated gamma power (arrow) in the striatum during quiet rest but not grooming and exploration. (B) Plots of mean coherence as a function of frequency (upper lane) and results of a statistical permutation test showing the probability of obtaining coherence values equal or larger than the observed values by chance. Data from quiet rest in WT (left) and HD (right). Highly significant coherence ($p < 0.001$) is found in the low gamma frequency range between 33 and 42 Hz (shaded column) in HD but not in WT. Pooled data from 5 WT and 3 HD mice.

cytoplasmic part of the soma and the average intensity was measured. One hundred and five cells from two animals per genotype were evaluated (Fig. 8B). Indeed, in the 1-year-old Q175 HOMs DARPP-32 immunofluorescence was significantly decreased and amounted to only 63.5% of the WT level. Nonetheless, DARPP-32+ somata could still be detected which allowed us to find out whether SPN numbers were starting to differ between WT and HD. This was not the case (Fig. 8C).

Decreased number of VGLUT1-immunofluorescent synaptic terminals in Q175 homozygotes

The presence of VGLUT1 is regarded as a reliable identification criterion for synaptic terminals of cortical origin since thalamostriatal afferents contain VGLUT2 (Deng et al., 2013). Fig. 9A presents high magnification overlay images from sections stained with the antibody combination VGLUT1/Syp/DARPP-32. Glutamatergic boutons appear in yellow-orange. The quantification of

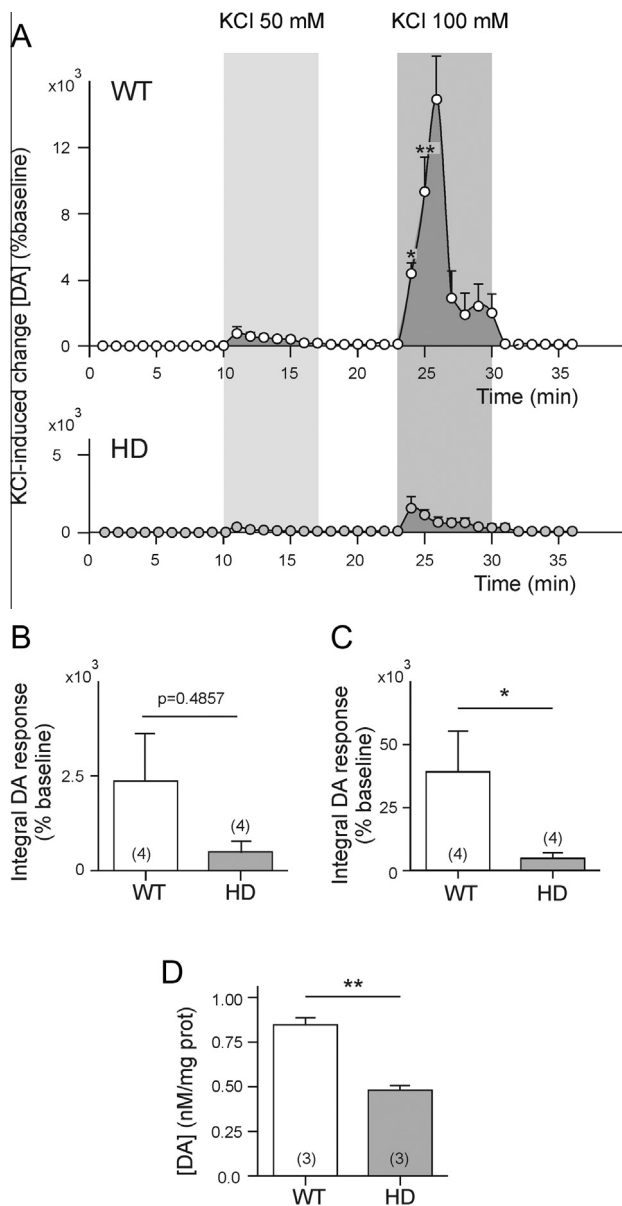


Fig. 6. Deficiency of KCl-induced release of dopamine (DA) in intact awake HD mice. Data from 4 WT and 4 Q175 HOMs of same sex (male) and similar age (58–59 weeks). (A) Microdialysis probes were implanted in the dorsal striatum and also used for a standard protocol of KCl-induced depolarization. The KCl-induced DA responses were determined by microdialysis and HPLC from samples collected during successive 10-min time periods. In each test the DA concentration was normalized to the average from eight control values prior to the first KCl application (= “baseline [DA] level”). Concentration levels larger than control mean plus 2 SD were qualified as part of the integral DA response to elevated KCl (darker shaded area). (B, C) The integral DA response was defined as the sum of suprathreshold [DA] values normalized to baseline level. About three trials were obtained per animal. The numbers in brackets indicate the numbers of tested animals. Responses to 50 mM KCl (B) and to 100 mM KCl (C). The p value in C was 0.0286. (D) Striatal dopamine concentration from striatal tissue punches in frozen sections. * $p < 0.05$, ** $p < 0.01$, Mann–Whitney U tests.

results from 3 WT and 3 HD mice (Fig. 9B) revealed a highly significant decrease in the number of VGLUT1-immunoreactive synaptic terminals. The absolute numbers are given in Table 1.

The loss of VGLUT1-positive synaptic terminals might cause an imbalance of excitatory (E) vs. inhibitory (I) synaptic input, unless the number of GABAergic synaptic terminals were reduced as well. To explore this possibility, alternating sections from the same animals were stained with the antibody combination VGAT/Syp/DARPP-32 (Fig. 9A, lower panel). The boutons in direct contact with a DARPP-32+ soma and the remaining boutons in the neuropil were quantified separately. In line with previous studies of GABAergic afferents to SPNs (Tepper et al., 2008) we assumed that GABAergic synaptic terminals on the soma were preferentially derived from parvalbumin-positive fast spiking interneurons. In contrast to other interneurons in the striatum, parvalbuminergic interneurons are afflicted by HD (Reiner et al., 2013). The counts from Q175 mice showed, indeed, that HD preferentially affected the numbers of GABAergic terminals in contact with the soma (Fig. 9B). The absolute numbers are given in Table 1. In contrast, no significant difference was found in the GAT+ terminals of the neuropil. Finally, the average E/I ratio of synaptic terminal numbers was calculated for each animal. The respective values were 0.8, 1.2, 1.3 (WT) and 0.8, 0.9, 0.9 (HD). It seems that at this hypokinetic stage of HD an imbalance of glutamatergic vs. GABAergic synaptic input might develop, but a larger cohort is needed to verify this possibility.

To summarize, about one fifth of corticostriatal VGLUT1-positive synaptic terminals were lost without noticeable deficits in the number of SPNs and their GABAergic synapses in the neuropil. Is this structural deficit matched by a corresponding decrease of AMPAR-mediated EPSCs? Patch-clamp recordings from functionally identified unitary corticostriatal connections were conducted to answer this question.

Reduced strength of unitary glutamatergic synaptic input to SPNs in HD

The release characteristics of individual cortical afferents to SPNs have not yet been determined directly as it is difficult to perform simultaneous recordings from connected cortical pyramidal neurons and SPNs. Indirect information was provided for HD mice by recording the composite responses to electrical stimulation of multiple neurons in the cerebral cortex (Joshi et al., 2009) or spontaneous glutamatergic EPSCs in the absence and presence of TTX (Cepeda et al., 2003, 2010; Plotkin et al., 2014; Indersmitten et al., 2015). Recently, single spine responses to channel rhodopsin stimulation were elicited in TTX which revealed a distinct feature of corticostriatal as opposed to thalamostriatal afferents, the TrkB-dependent postsynaptic potentiation (Plotkin et al., 2014). This mechanism was seriously compromised in HD, notably in iSPNs.

To further expand the present knowledge on glutamatergic synaptic transmission in the striatum, we have analyzed AMPA-receptor-mediated postsynaptic responses with a distinct activation threshold at minimal current intensity. Responses to other neurotransmitters were blocked pharmacologically. To make the present data set more homogenous we selected glutamatergic

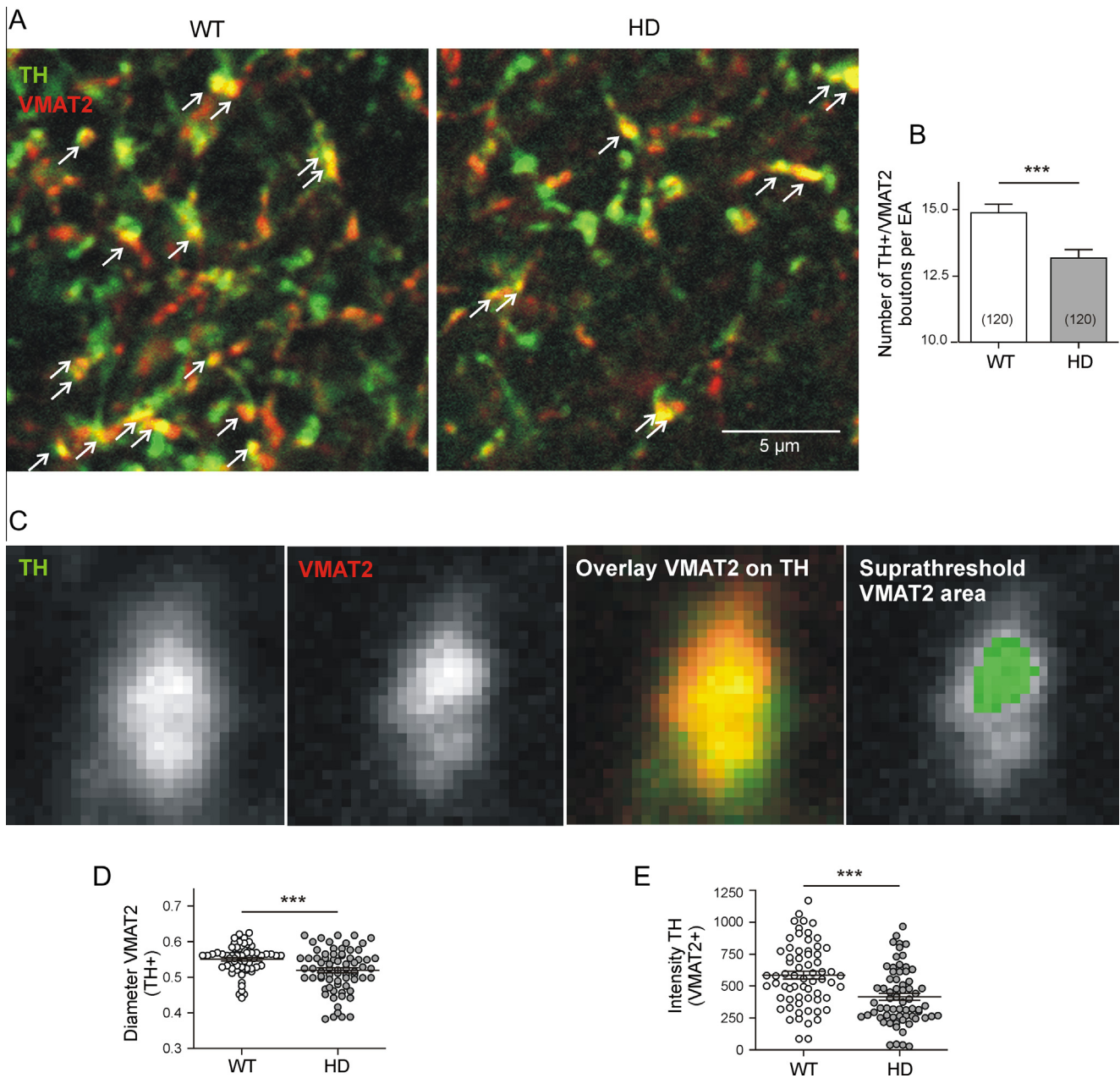


Fig. 7. HD-related loss of dopaminergic synaptic terminals and reduced level of TH immunofluorescence in VMAT2-positive synaptic terminals (red). (A) Evaluation areas in the dorsal striatum of WT and HD mice after immunolabeling of TH (green) and VMAT2 (red). Arrowheads denote double-stained varicosities, i.e. presumed dopaminergic synaptic terminals. (B) Counts show a significant reduction in the number of VMAT2 +/TH+ synaptic varicosities in HD. (C) A ROI of $1.875 \times 1.875 \mu\text{m}$ containing one bouton only for detailed quantification. Last in the panel: Calculated presynaptic VMAT2 area (green) of a TH+ spot (white), as determined by setting the intensity threshold in the VMAT2 channel = mean + 2.5 SD. (D) HD-related difference in the calculated mean diameter of the VMAT2 +/TH+ spots. (E) Mean TH fluorescence intensity of VMAT2 + spots. a.u., arbitrary units. Symbols: *** $p < 0.001$. Mann–Whitney U -test (B, D, E), n , number of EAs (B) or number of analysed ROIs (D, E). (For interpretation of the references to color in this figure legend, the reader is referred to the web version of this article.)

EPSCs with PPF. Previous studies have established PPF as a functional marker of corticostriatal afferents (Ding et al., 2008). In contrast, thalamostriatal afferents were shown to display paired-pulse depression (PPD). Under the present conditions axons exhibiting PPF were encountered relatively seldom (only two out of 10 tested sites) which unfavorably added to the recording time needed for verification of the unitary character of the postsynaptic response. However, in case of successful search

(Fig. 10A–C) one could obtain a reliable indicator of synaptic coupling between just one presynaptic and one postsynaptic neuron, as already demonstrated by a previous study of uEPSCs in response to subthalamo-nigral afferents (Dvorzhak et al., 2013a).

The specific aim of the present analysis of uEPSCs of presumed cortical origin was to explore the regulatory range of glutamatergic synaptic transmission based on the values of the three largest EPSCs (EPSC_{max}) within

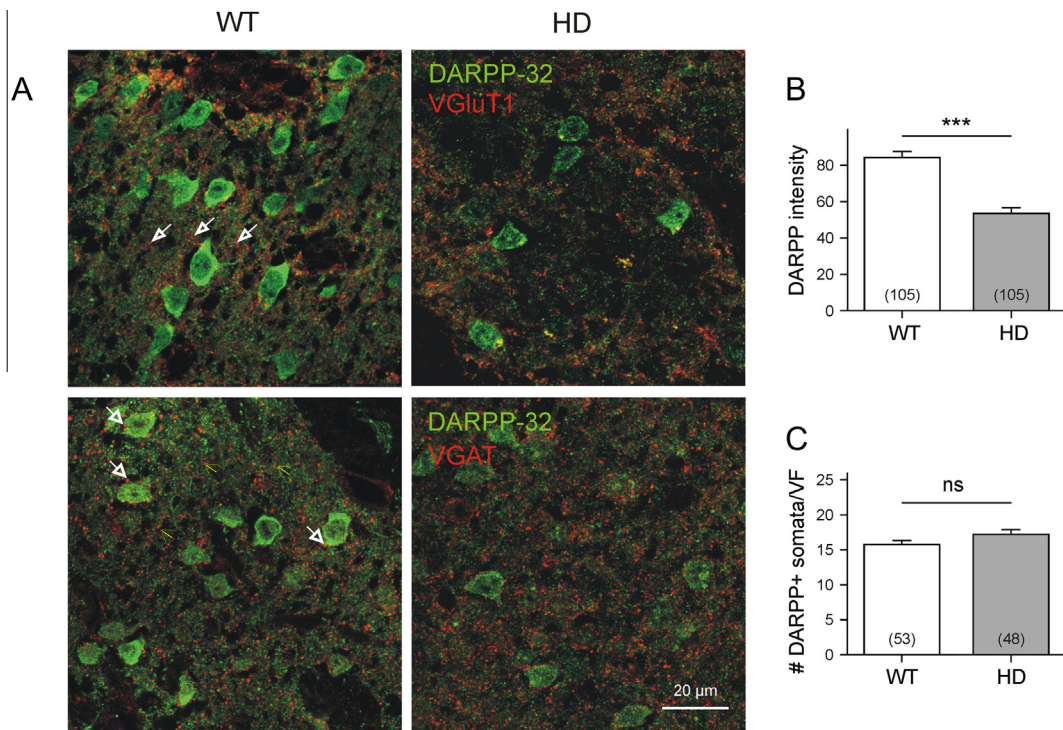


Fig. 8. Reduced DARPP-32 immunoreactivity but unchanged numbers of striatal output neurons in HD. (A) Viewfields in the dorsal striatum showing weaker DARPP-32 immunofluorescence (green) in HD. The red channel shows VGlut1 (upper panel) and VGAT (lower panel). The arrowheads refer to three types of varicosities: VGlut1+ (upper panel), VGAT+ in contact with soma (lower panel, white) and VGAT+ in the neuropil (lower panel, yellow). (B) Quantification of somatic extranuclear fluorescence intensity of DARPP-32 in single SONs. In brackets: Number of cells. Mann–Whitney test. ***Difference significant at $p < 0.001$. (C) Counts of DARPP-32+ neurons in the dorsal striatum. In brackets: Number of viewfields. Unpaired t -test. n.s., not significant. (For interpretation of the references to color in this figure legend, the reader is referred to the web version of this article.)

a series of 120 paired stimulations (Fig. 10D) under conditions that would minimize the impact of presynaptic modulatory mechanisms. To abolish the presynaptic G-protein-dependent modulation of glutamate release, a G protein alkylating agent, NEM was added to the bath solution for a period of 15 min before acquiring the test EPSCs (Kirmse and Kirischuk, 2006). At a concentration of 50 μ M, NEM strongly increased the release probability which resulted in a reduced failure rate (Table 1) and larger values of average (not shown) and maximal EPSC amplitudes (Fig. 10A, Table 1). Furthermore, after 15 min of NEM exposure all connections switched from PPF to PPD. The threshold toggling procedure was then repeated to ensure that the response has remained unitary before proceeding with the records and the search for the three maximal responses (Fig. 10D).

In the absence of presynaptic modulatory mechanisms, the maximal EPSC amplitudes should correlate with the number of transmitter releasing sites, as demonstrated in various synaptic connections where morphological reconstructions were performed in addition to sampling fluctuating PSCs (for instance (Redman and Walmsley, 1983; Grantyn et al., 1984)). Our experiments show, for the first time, that the uEPSCs of presumed cortical origin differed significantly in an HD-related manner (Fig. 10E). Smaller response maxima indicate a reduced dynamic range of the corticostriatal input in HD, most likely as a consequence of the reduced number of release sites per connection.

DISCUSSION

Hypokinesia in Q175 mice

The starting point of this study was the observation that Q175 homozygotes exhibited signs of hypokinesia, especially when tested during day-light. The term hypokinesia refers to impairment of movement initiation due to difficulty selecting and/or activating respective motor programs in the basal ganglia. Based on the comparison of WT and Q175 HOMs we have interpreted the following observations as signs of hypokinesia: Reduced number of spontaneous movements on a balance after exposure to light (−55%), increased total time spent without movement (+42%), failures in the execution of unconditioned avoidance reactions (+32%), reduced ability for conditioned avoidance (−96%) and increased reaction times (+65%). The summarizing Table 1 shows the respective values.

Temel and colleagues (Jahanshahi et al., 2010) forwarded the opinion that in contrast to his rat model of HD most of the common HD mice exhibit neurodegeneration without chorea. This might be correct but does not diminish the value of the present-day knock-in models of HD, since in humans hypokinesia and dystonia invariably occur, becoming dominant in grade 2–3 HD (Donaldson et al., 2012; Ross et al., 2014). The respective motor impairment score is the best predictor of neuropathological severity (Rosenblatt et al., 2003).

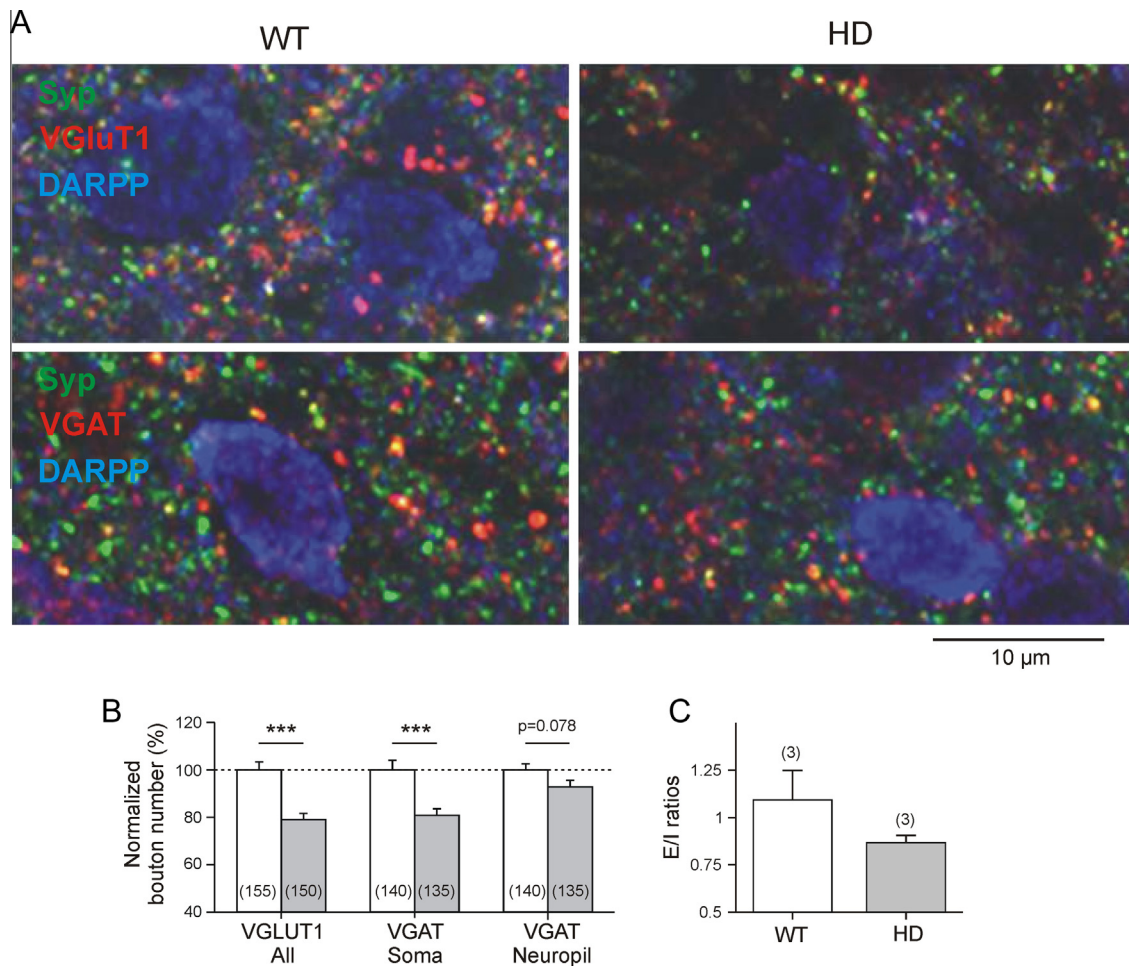


Fig. 9. Loss of glutamatergic (upper panel red) and GABAergic (lower panel red) synaptic terminals in Q175 HOMs. (A) High magnification confocal fluorescent images (overlay) from Q175 WT and HOM. (B) Results of bouton counts. The data were normalized to the wild type average. In brackets: Number of circular evaluation areas (diameter 30 μ m). Mann–Whitney test (VGLUT1) and unpaired *t*-test (VGAT soma). ***Difference between means significant at $p < 0.001$. Pooled results from 3 WT and 3 HD mice. (C) Ratios of average VGLUT1/VGAT numbers from 3 animals per genotype. (For interpretation of the references to color in this figure legend, the reader is referred to the web version of this article.)

Our present results are consistent with failure of dopaminergic and glutamatergic synaptic transmission as a basis for motor impairment in Huntington mice with hypokinesia. We found a massive reduction of KCl-induced dopamine release in awake mice (–89%), a decrease in the number of TH+/VMAT+ synaptic terminals in the dorsal striatum (–11%), a reduction in the presynaptic TH fluorescence intensity (–29%), a decrease in the somatic DARPP-32 fluorescence (–37%), but no decrease in the number of DARPP-32+ cells per view field. In addition there was a marked loss of VGluT1+ synaptic terminals (–31%) and a reduction in the maximal amplitudes of nonmodulated EPSCs. This argues against the idea that hypokinesia in advanced HD primarily reflects the degeneration of dSPNs and supports the hypothesis of failing dopaminergic control and structural impairment of the corticostriatal pathway.

Reduced dopamine release in Q175 mice

The detailed mechanisms of dopaminergic modulation of corticostriatal coupling are complex and differ in D1 and

D2 expressing SPNs (Surmeier et al., 2014). Among other possibilities, symptoms of striatal dopamine insufficiency in advanced HD could be caused by the following alterations: loss of dopaminergic synaptic terminals (Bohnen et al., 2000; Bedard et al., 2011), impairment of dopamine uptake (Ginovart et al., 1997; Bohnen et al., 2000) and loss of D1 and D2 receptors (Cha et al., 1998; Pavese et al., 2003; Crook and Housman, 2012). Dopamine depletion in the striatum could produce (i) alterations in SPN excitability leading to pathological pacemaker activity and increased entrainment of unitary discharge to LFP waveforms (Burkhardt et al., 2009), (ii) reduced dopaminergic facilitation of corticostriatal connections with D1-expressing direct SPNs due to impaired interaction with NMDA receptors (Murphy et al., 2014) and/or (iii) disinhibition of glutamate release from corticostriatal terminals on D2-expressing indirect SPNs due to impaired activation of the mGluR5/CB1 signaling pathway (Lerner and Kreitzer, 2012). This list is incomplete and it is obvious, that the present experimental results cannot clarify any of these mechanisms but merely provide quantitative estimates characterizing the state of the dopaminergic system in the dorsal striatum of Q175 homozygotes vs. WT mice.

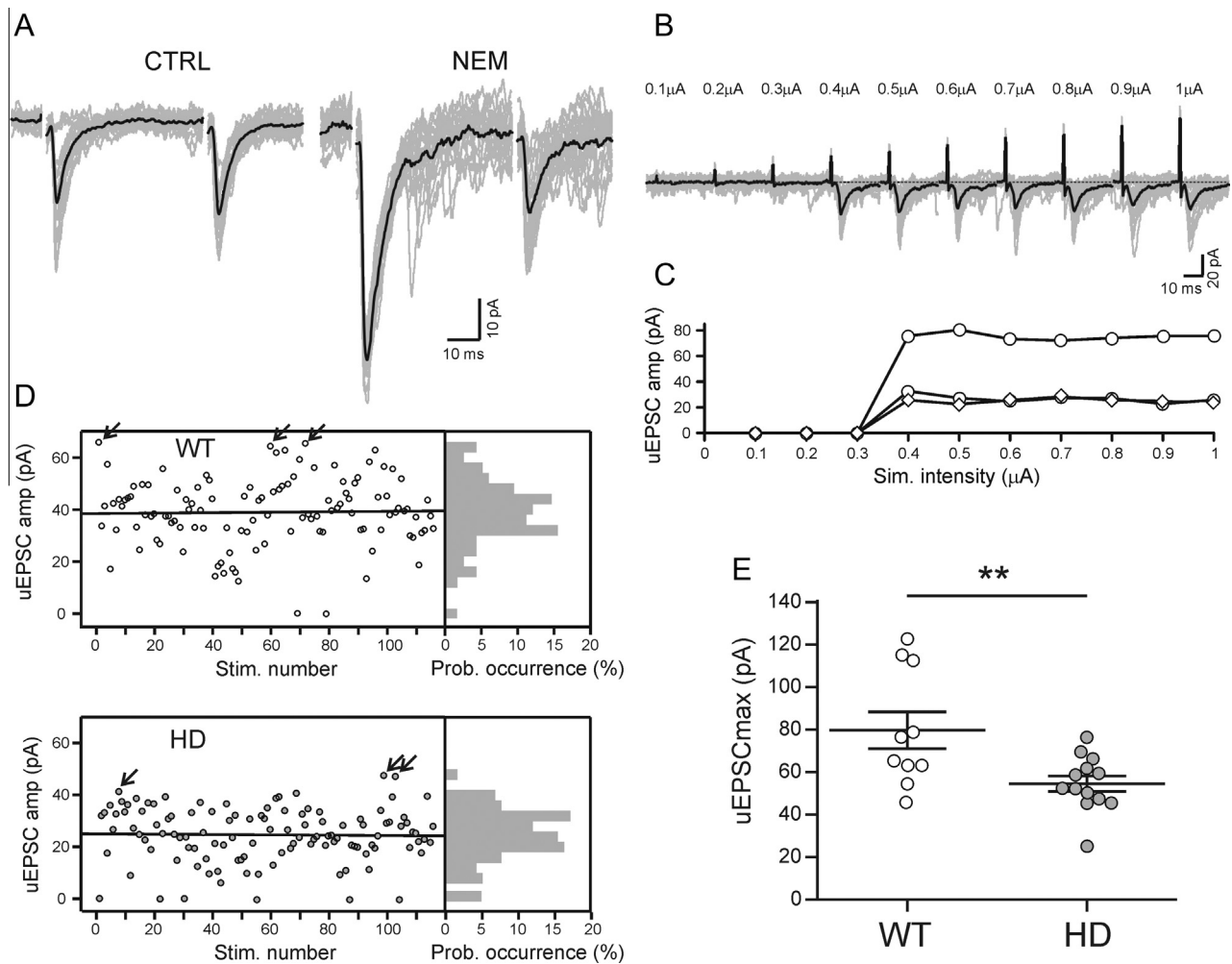


Fig. 10. Decreased dynamic range in unitary glutamatergic synaptic transmission in the striatum of HD mice. (A) Specimens of superimposed EPSCs in Control (CTRL) and in the presence of the G-Protein blocker NEM (50 μ M). Note NEM-induced transition from PPF to PPD. Gray – individual responses, black – average traces. (B, C) Threshold toggling in three different units. The graph shows average amplitudes. (D) Plot of 1st uEPSC amplitudes in NEM against stimulus number to illustrate fluctuations in WT and HD. The arrows point to the three largest uEPSCs as used for estimation of uEPSCmax. On the right: Amplitude histograms in 4 pA bins. (E) Maximal uEPSC amplitudes (i.e. average of three largest events from each cell) in WT and HD. ** $p < 0.01$, Mann–Whitney test.

Our results from awake animals are in line with previous voltammetric data from striatal slices of R6/1 or R6/2 mice (Petersen et al., 2002; Johnson et al., 2006; Dallerac et al., 2015) and *in vivo* microdialysis in R6/2 and YAC128 mice (Callahan and Abercrombie, 2011). Among the possible causes of reduced KCl-induced dopamine release one may consider compromised re-uptake reducing the filling state of vesicles and/or reduced synapse density. Johnson et al. (2006) reported no HD-related difference in dopamine uptake, but evidence for reduced dopaminergic innervation of the dorsal striatum has already been found (Ariano et al., 2002). Optical density quantification of TH immunoreactivity showed a decrease similar to that of PD patients (Bedard et al., 2011). The reduction in striatal tissue dopamine concentration, as shown here, would be compatible with the latter two possibilities. Our evaluation of individual double-labeled axon terminals provide strong evidence for both reduced terminal density and reduced TH levels at VMAT2-positive presynaptic sites.

Whether or not hypokinesia in HD is caused or accompanied by neuron loss in the *substantia nigra pars compacta* is currently not known.

Hypokinesia in combination with a deficiency of striatal dopamine release makes the Q175 homozygotes to some extent Parkinson-like, which raises the question whether some other landmarks of PD were shared with HD. In studies of advanced PD, hypokinesia was shown to correlate with the appearance of L-DOPA-sensitive pathological beta-band (8–30 Hz) oscillations in the pallido-subthalamic network (Brown, 2003). In the striatum of DA-deprived rats oscillations were found as well, but in this case mostly in the gamma band (Lemaire et al., 2012). Interestingly, these oscillations appeared to be task-specific.

Rebec and colleagues (Miller et al., 2011) made the important discovery that state-dependent striatal oscillations in the low gamma range (frequencies between 33 and 42 Hz, peak at 37 Hz) accompany HD in R6/2 mice.

These oscillations only appeared in the absence of motor activity (Miller et al., 2011; Hong et al., 2012) and associated with a tendency for burst generation in single unit recordings (Miller et al., 2011). It is conceivable that spontaneous synchronized activity in the striatum at rest can affect the probability of movement execution on the background of such pathological resting state (Gonzalez Andino et al., 2005; Oswal et al., 2012; von Nicolai et al., 2014). Spontaneously active SPNs would discriminate an incoming signal from the motor cortex with less precision (Shirendeb et al., 2012), since a hyperpolarized state of the SPNs near the *K* equilibrium potential (“down state”) is the requirement for a sharp transition to the “up state”, when the glutamatergic input from the cerebral cortex reaches a critical level (Plotkin et al., 2011).

The source of the pathological gamma oscillations at rest needs to be determined. Since in bipolar LFP recordings gamma oscillations were more prominent in the striatum than in the motor cortex, one may tentatively assume that the pacemaker is localized in the striatum itself. Gamma oscillations in the EEG recordings from the cortex of HD patients are not reported. The most prominent feature in human HD was the depression of alpha and beta power (see (Nguyen et al., 2010) for a comprehensive review). Disease progression was associated with a general slowing of cortical rhythms presumably reflecting decreased vigilance (enhanced delta/theta power) and impairment of cognitive/motor activity (decreased alpha and beta power).

Alterations in corticostriatal glutamatergic synaptic transmission

We report that in symptomatic Q175 homozygotes the number of VGLUT1-positive terminals dropped to 69% of WT level, and this was accompanied by a similar decrease (–31%) in the functional range of presumed corticostriatal synaptic transmission. In view of the unchanged SPN numbers in the counts of immunostained DARPP-32 neurons, the loss of striatal volume may be attributed to changes in the neuropil. That loss of axons terminals could precede the death of SPNs has been suggested by data from other mouse models of HD (Deng et al., 2013, 2014; Naydenov et al., 2014; Marangoni et al., 2014). It was even proposed that *htt* mutation could compromise the development of corticostriatal connections during postnatal ontogeny (McKinstry et al., 2014). The reduction in the number of VGLT1+ terminals is in line with the studies reporting a substantial decrease in the number of spines on SPNs (Plotkin et al., 2014; Indersmitten et al., 2015). Specific estimates are available for direct vs. indirect SPNs. In 6–8 months old BACHD mice the spine density was only reduced in indirect SPNs (Plotkin et al., 2014) which supported the hypothesis that early in HD iSPNs exhibit a higher vulnerability (Reiner et al., 1988; Sapp et al., 1995; Glass et al., 2000; Deng et al., 2004). In Q140 KI mice premanifest motor slowing was primarily associated with loss of cortical afferents to dSPNs (Deng et al., 2014).

Still missing is detailed information on the functional deficits in corticostriatal synaptic transmission. Multi-unit activation of corticostriatal afferents by electrical

stimulation in the motor cortex is not well suited to clarify the site of deficit. HD-related differences in response amplitudes only appear at higher stimulation intensities (Joshi et al., 2009), when current spread to the striatum is likely to occur. For the time being it therefore seemed more promising to use the PPF-criterion of Surmeier and colleagues (Ding et al., 2008) to select corticostriatal afferents for minimal stimulation experiments, as described before (Dvorzhak et al., 2013a,b). Of particular interest were possible changes in the regulatory range of individual corticostriatal connections. In this context we wanted to know whether a single corticostriatal afferent could drive an SPN from a “down state” to an “up state”. The number of spines required for this transition has recently been determined and it is relatively small, about 12 on average (Plotkin and Surmeier, 2015). Could such number of contacts be formed by an individual unitary connection between one presynaptic and one postsynaptic cell? The tentative answer obtained from the present recordings of uEPSCs is: yes. In WT mice the average size of unmodulated uEPSCs (79 pA) is compatible with the activation of 11–16 spines, as determined by measuring the size of somatic EPSCs recorded after single spine uncaging on distal dendrites (Plotkin et al., 2014) and estimating the quantal steps in responses to glutamate uncaging on dendritic spines of WT SPNs (Dvorzhak and Grantyn, unpublished observation). However, this approach still lacks criteria to separate glutamatergic inputs of cortical and thalamic origin.

To resolve the maximal quantal content of uEPSCs for comparison of WT and HD mice is not an easy task and requires a number of conditions to be fulfilled. First of all, it is necessary to exclude the possibly existing HD-related differences in the modulation of release via tonically active presynaptic CB1, A2 or D2 receptors. The latter might be affected by HD which could influence the chance of recording the response maximum, i.e. the functional equivalent to activation of all release sites belonging to the unitary connection. We therefore recorded the fluctuating uEPSCs in NEM, a broad-band blocker of G-protein signaling. The experiments suggest that in HD individual corticostriatal afferents may indeed form fewer contacts. The percent decrease in the maximal amplitudes of uEPSCs was similar to the loss of VGLUT1 terminals (–31%). A reduction of that amount must be regarded as a serious alteration especially if combined with a reduced number of functional AMPA receptors on the postsynaptic side of the still functional synapses (Plotkin et al., 2014).

What could be the main course of synapse loss in an existing synaptic connection? In view of results underlining the potency of homeostatic regulation in synaptic transmission (Turrigiano, 2008) one may consider the influence of impaired glutamate uptake by striatal astrocytes in HD (Estrada-Sanchez and Rebec, 2012). Delayed or insufficient clearance of synaptically released glutamate may lead to a downregulation of AMPA receptors in the synaptic cleft which in its turn could destabilize terminals attached to such sites. Further experiments with experimental rescue of GLT-1 may provide an answer to this question.

CONCLUSION

Our results suggest that restoring synaptic dopamine and glutamate release should normalize striatal activity at rest, abolish pathological gamma oscillations and alleviate the symptom of hypokinesia.

Acknowledgment—This work is supported by the Cure Huntington's Disease Initiative foundation (A-7815), the German Research Council (Gr986/10-1, Exc 257/1), Charité Research Funds (2015-040) and intramural funds of the Leibniz Institute of Neurobiology. We highly appreciate the expert advice of Dr. Hannes Schmidt at the Max Delbrück Center for Molecular Medicine Berlin and Dr. Svetlana Warton, retired from the University of Sydney. Jörg Rösner at the Neurocure Microscope Core Facility provided skilled technical assistance.

REFERENCES

- Albin RL, Young AB, Penney JB (1989) The functional anatomy of basal ganglia disorders. *Trends Neurosci* 12:366–375.
- Anderson KD, Reiner A (1991) Immunohistochemical localization of DARPP-32 in striatal projection neurons and striatal interneurons: implications for the localization of D1-like dopamine receptors on different types of striatal neurons. *Brain Res* 568:235–243.
- Andre VM, Cepeda C, Levine MS (2010) Dopamine and glutamate in Huntington's disease: a balancing act. *CNS Neurosci Ther* 16:163–178.
- Ariano MA, Aronin N, DiFiglia M, Tagle DA, Sibley DR, Leavitt BR, Hayden MR, Levine MS (2002) Striatal neurochemical changes in transgenic models of Huntington's disease. *J Neurosci Res* 68:716–729.
- Bateup HS, Santini E, Shen W, Birnbaum S, Valjent E, Surmeier DJ, Fissone G, Nestler EJ, Greengard P (2010) Distinct subclasses of medium spiny neurons differentially regulate striatal motor behaviors. *Proc Natl Acad Sci U S A* 107:14845–14850.
- Bedard C, Wallman MJ, Pouchet E, Gould PV, Parent A, Parent M (2011) Serotonin and dopamine striatal innervation in Parkinson's disease and Huntington's chorea. *Parkinsonism Relat Disord* 17:593–598.
- Bibb JA, Yan Z, Svenningsson P, Snyder GL, Pieribone VA, Horiuchi A, Nairn AC, Messer A, Greengard P (2000) Severe deficiencies in dopamine signaling in presymptomatic Huntington's disease mice. *Proc Natl Acad Sci U S A* 97:6809–6814.
- Bohnen NI, Koeppe RA, Meyer P, Fieco E, Wernette K, Kilbourn MR, Kuhl DE, Frey KA, Albin RL (2000) Decreased striatal monoaminergic terminals in Huntington disease. *Neurology* 54:1753–1759.
- Brown P (2003) Oscillatory nature of human basal ganglia activity: relationship to the pathophysiology of Parkinson's disease. *Mov Disord* 18:357–363.
- Burkhardt JM, Jin X, Costa RM (2009) Dissociable effects of dopamine on neuronal firing rate and synchrony in the dorsal striatum. *Front Integr Neurosci* 3:28.
- Callahan JW, Abercrombie ED (2011) In vivo dopamine efflux is decreased in striatum of both fragment (R6/2) and full-length (YAC128) transgenic mouse models of Huntington's disease. *Front Syst Neurosci* 5:61.
- Cepeda C, Cummings DM, Hickey MA, Kleiman-Weiner M, Chen JY, Watson JB, Levine MS (2010) Rescuing the corticostriatal synaptic disconnection in the R6/2 mouse model of Huntington's disease: exercise, adenosine receptors and ampkines. *PLoS Curr*:RRN1182.
- Cepeda C, Hurst RS, Calvert CR, Hernandez-Echeagaray E, Nguyen OK, Jocoy E, Christian LJ, Ariano MA, Levine MS (2003) Transient and progressive electrophysiological alterations in the corticostriatal pathway in a mouse model of Huntington's disease. *J Neurosci* 23:961–969.
- Cepeda C, Murphy KP, Parent M, Levine MS (2014) The role of dopamine in Huntington's disease. *Prog Brain Res* 211:235–254.
- Cepeda C, Wu N, Andre VM, Cummings DM, Levine MS (2007) The corticostriatal pathway in Huntington's disease. *Prog Neurobiol* 81:253–271.
- Cha JH, Kosinski CM, Kerner JA, Alsdorf SA, Mangiarini L, Davies SW, Penney JB, Bates GP, Young AB (1998) Altered brain neurotransmitter receptors in transgenic mice expressing a portion of an abnormal human huntington disease gene. *Proc Natl Acad Sci U S A* 95:6480–6485.
- Crook ZR, Housman DE (2012) Dysregulation of dopamine receptor D2 as a sensitive measure for Huntington disease pathology in model mice. *Proc Natl Acad Sci U S A* 109:7487–7492.
- Dallerac GM, Levasseur G, Vatsavayi SC, Milnerwood AJ, Cummings DM, Kraev I, Huetz C, Evans KA, Walters SW, Rezaie P, Cho Y, Hirst MC, Murphy KP (2015) Dysfunctional dopaminergic neurons in mouse models of Huntington's disease: a role for SK3 channels. *Neurodegener Dis* 15:93–108.
- Deng YP, Albin RL, Penney JB, Young AB, Anderson KD, Reiner A (2004) Differential loss of striatal projection systems in Huntington's disease: a quantitative immunohistochemical study. *J Chem Neuroanat* 27:143–164.
- Deng YP, Wong T, Bricker-Anthony C, Deng B, Reiner A (2013) Loss of corticostriatal and thalamostriatal synaptic terminals precedes striatal projection neuron pathology in heterozygous Q140 Huntington's disease mice. *Neurobiol Dis* 60:89–107.
- Deng YP, Wong T, Wan JY, Reiner A (2014) Differential loss of thalamostriatal and corticostriatal input to striatal projection neuron types prior to overt motor symptoms in the Q140 knock-in mouse model of Huntington's disease. *Front Syst Neurosci* 8:198.
- Ding J, Peterson JD, Surmeier DJ (2008) Corticostriatal and thalamostriatal synapses have distinctive properties. *J Neurosci* 28:6483–6492.
- Donaldson I, Marsden C.D., Schneider S.A., Bhatia KP (2012) *Huntington's Disease*. pp 733–784. Oxford University Press.
- Dvorzhak A, Gertler C, Hamack D, Grantyn R (2013a) High frequency stimulation of the subthalamic nucleus leads to presynaptic GABA(B)-dependent depression of subthalamic afferents. *PLoS One* 8:e82191.
- Dvorzhak A, Semtner M, Faber DS, Grantyn R (2013b) Tonic mGluR5/CB1-dependent suppression of inhibition as a pathophysiological hallmark in the striatum of mice carrying a mutant form of huntingtin. *J Physiol* 591:1145–1166.
- Estrada-Sanchez AM, Rebec GV (2012) Corticostriatal dysfunction and glutamate transporter 1 (GLT1) in Huntington's disease: interactions between neurons and astrocytes. *Basal Ganglia* 2:57–66.
- Ginovart N, Lundin A, Farde L, Halldin C, Backman L, Swahn CG, Pauli S, Sedvall G (1997) PET study of the pre- and post-synaptic dopaminergic markers for the neurodegenerative process in Huntington's disease. *Brain* 120:503–514.
- Glass M, Dragunow M, Faull RL (2000) The pattern of neurodegeneration in Huntington's disease: a comparative study of cannabinoid, dopamine, adenosine and GABA(A) receptor alterations in the human basal ganglia in Huntington's disease. *Neurosci* 97:505–519.
- Gonzalez Andino SL, Michel CM, Thut G, Landis T, Grave DP (2005) Prediction of response speed by anticipatory high-frequency (gamma band) oscillations in the human brain. *Hum Brain Mapp* 24:50–58.
- Grantyn R, Shapovalov AI, Shiriaev BI (1984) Relation between structural and release parameters at the frog sensory-motor synapse. *J Physiol* 349:459–474.
- Heikkinen T, Lehtimäki K, Vartiainen N, Puolivali J, Hendricks SJ, Glaser JR, Bradaia A, Wadel K, Touller C, Kontkanen O, Yrjanheikki JM, Buisson B, Howland D, Beaumont V, Muñoz-Sanjuan I, Park LC (2012) Characterization of neurophysiological and behavioral changes, MRI brain volumetry and 1H MRS in zQ175 knock-in mouse model of Huntington's disease. *PLoS One* 7:e50717.

- Henneberger C, Kirischuk S, Grantyn R (2005) Brain-derived neurotrophic factor modulates GABAergic synaptic transmission by enhancing presynaptic glutamic acid decarboxylase 65 levels, promoting asynchronous release and reducing the number of activated postsynaptic receptors. *Neurosci* 135:749–763.
- Hong SL, Cossyleon D, Hussain WA, Walker LJ, Barton SJ, Rebec GV (2012) Dysfunctional behavioral modulation of corticostriatal communication in the R6/2 mouse model of Huntington's disease. *PLoS One* 7:e47026.
- Indersmitten T, Tran CH, Cepeda C, Levine MS (2015) Altered excitatory and inhibitory inputs to striatal medium-sized spiny neurons and cortical pyramidal neurons in the Q175 mouse model of Huntington's disease. *J Neurophysiol* 113:2953–2966.
- Jahanshahi A, Vlamings R, Kaya AH, Lim LW, Janssen ML, Tan S, Visser-Vandewalle V, Steinbusch HW, Temel Y (2010) Hyperdopaminergic status in experimental Huntington disease. *J Neuropathol Exp Neurol* 69:910–917.
- Johnson MA, Rajan V, Miller CE, Wightman RM (2006) Dopamine release is severely compromised in the R6/2 mouse model of Huntington's disease. *J Neurochem* 97:737–746.
- Joshi PR, Wu NP, Andre VM, Cummings DM, Cepeda C, Joyce JA, Carroll JB, Leavitt BR, Hayden MR, Levine MS, Bamford NS (2009) Age-dependent alterations of corticostriatal activity in the YAC128 mouse model of Huntington disease. *J Neurosci* 29:2414–2427.
- Kirmse K, Kirischuk S (2006) N-ethylmaleimide increases release probability at GABAergic synapses in layer I of the mouse visual cortex. *Eur J Neurosci* 24:2741–2748.
- Kita T, Kita H, Kitai ST (1984) Passive electrical membrane properties of rat neostriatal neurons in an in vitro slice preparation. *Brain Res* 300:129–139.
- Lemaire N, Hernandez LF, Hu D, Kubota Y, Howe MW, Graybiel AM (2012) Effects of dopamine depletion on LFP oscillations in striatum are task- and learning-dependent and selectively reversed by L-DOPA. *Proc Natl Acad Sci U S A* 109:18126–18131.
- Lerner TN, Kreitzer AC (2012) RGS4 is required for dopaminergic control of striatal LTD and susceptibility to parkinsonian motor deficits. *Neuron* 73:347–359.
- Loh DH, Kudo T, Truong D, Wu Y, Colwell CS (2013) The Q175 mouse model of Huntington's disease shows gene dosage- and age-related decline in circadian rhythms of activity and sleep. *PLoS ONE* 8:e69993.
- Marangoni M, Adalbert R, Janeckova L, Patrick J, Kohli J, Coleman MP, Conforti L (2014) Age-related axonal swellings precede other neuropathological hallmarks in a knock-in mouse model of Huntington's disease. *Neurobiol Aging* 35:2382–2393.
- McKinstry SU, Karadeniz YB, Worthington AK, Hayrapetyan VY, Ozlu MI, Serafin-Molina K, Risher WC, Ustunkaya T, Dragatsis I, Zeitlin S, Yin HH, Eroglu C (2014) Huntingtin is required for normal excitatory synapse development in cortical and striatal circuits. *J Neurosci* 34:9455–9472.
- Menalled LB, Kudwa AE, Miller S, Fitzpatrick J, Watson-Johnson J, Keating N, Ruiz M, Mushlin R, Alosio W, McConnell K, Connor D, Murphy C, Oakeshott S, Kwan M, Beltran J, Ghavami A, Brunner D, Park LC, Ramboz S, Howland D (2012) Comprehensive behavioral and molecular characterization of a new knock-in mouse model of Huntington's disease: zQ175. *PLoS ONE* 7:e49838.
- Miller BR, Walker AG, Barton SJ, Rebec GV (2011) Dysregulated neuronal activity patterns implicate corticostriatal circuit dysfunction in multiple rodent models of Huntington's disease. *Front Syst Neurosci* 5:26.
- Murphy JA, Stein IS, Lau CG, Peixoto RT, Aman TK, Kaneko N, Aromolaran K, Saulnier JL, Popescu GK, Sabatini BL, Hell JW, Zukin RS (2014) Phosphorylation of Ser1166 on GluN2B by PKA is critical to synaptic NMDA receptor function and Ca²⁺ signaling in spines. *J Neurosci* 34:869–879.
- Naydenov AV, Sepers MD, Swinney K, Raymond LA, Palmiter RD, Stella N (2014) Genetic rescue of CB1 receptors on medium spiny neurons prevents loss of excitatory striatal synapses but not motor impairment in HD mice. *Neurobiol Dis* 71:140–150.
- Nguyen L, Bradshaw JL, Stout JC, Croft RJ, Georgiou-Karistianis N (2010) Electrophysiological measures as potential biomarkers in Huntington's disease: review and future directions. *Brain Res Rev* 64:177–194.
- Nisenbaum ES, Wilson CJ (1995) Potassium currents responsible for inward and outward rectification in rat neostriatal spiny projection neurons. *J Neurosci* 15:4449–4463.
- Oswal A, Litvak V, Sauleau P, Brown P (2012) Beta reactivity, prospective facilitation of executive processing, and its dependence on dopaminergic therapy in Parkinson's disease. *J Neurosci* 32:9909–9916.
- Pavese N, Andrews TC, Brooks DJ, Ho AK, Rosser AE, Barker RA, Robbins TW, Sahakian BJ, Dunnett SB, Piccini P (2003) Progressive striatal and cortical dopamine receptor dysfunction in Huntington's disease: a PET study. *Brain* 126:1127–1135.
- Paxinos G, Franklin KBJ (2003) *The Mouse Brain in Stereotaxic Coordinates*. Elsevier.
- Perrotta A, Serpino C, Cormio C, Serrao M, Sandrini G, Pierelli F, de Tommaso M (2012) Abnormal spinal cord pain processing in Huntington's disease. The role of the diffuse noxious inhibitory control. *Clin Neurophysiol* 123:1624–1630.
- Petersen A, Puschban Z, Lotharius J, Nicnicocail B, Wiekop P, O'Connor WT, Brundin P (2002) Evidence for dysfunction of the nigrostriatal pathway in the R6/1 line of transgenic Huntington's disease mice. *Neurobiol Dis* 11:134–146.
- Plotkin JL, Day M, Peterson JD, Xie Z, Kress GJ, Rafalovich I, Kondapalli J, Gertler TS, Flajolet M, Greengard P, Stavarache M, Kaplitt MG, Rosinski J, Chan CS, Surmeier DJ (2014) Impaired TrkB receptor signaling underlies corticostriatal dysfunction in Huntington's disease. *Neuron* 83:178–188.
- Plotkin JL, Day M, Surmeier DJ (2011) Synaptically driven state transitions in distal dendrites of striatal spiny neurons. *Nat Neurosci* 14:881–888.
- Plotkin JL, Surmeier DJ (2015) Corticostriatal synaptic adaptations in Huntington's disease. *Curr Opin Neurobiol* 33C:53–62.
- Redman S, Walmsley B (1983) Amplitude fluctuations in synaptic potentials evoked in cat spinal motoneurons at identified group Ia synapses. *J Physiol* 343:135–145.
- Reiner A, Albin RL, Anderson KD, D'Amato CJ, Penney JB, Young AB (1988) Differential loss of striatal projection neurons in Huntington disease. *Proc Natl Acad Sci U S A* 85:5733–5737.
- Reiner A, Shelby E, Wang H, Demarch Z, Deng Y, Guley NH, Hogg V, Roxburgh R, Tippett LJ, Waldvogel HJ, Faull RL (2013) Striatal parvalbuminergic neurons are lost in Huntington's disease: implications for dystonia. *Mov Disord* 28:1691–1699.
- Rosenblatt A, Abbott MH, Gourley LM, Troncoso JC, Margolis RL, Brandt J, Ross CA (2003) Predictors of neuropathological severity in 100 patients with Huntington's disease. *Ann Neurol* 54:488–493.
- Ross CA, Aylward EH, Wild EJ, Langbehn DR, Long JD, Warner JH, Scahill RI, Leavitt BR, Stout JC, Paulsen JS, Reilmann R, Unschuld PG, Wexler A, Margolis RL, Tabrizi SJ (2014) Huntington disease: natural history, biomarkers and prospects for therapeutics. *Nat Rev Neurol* 10:204–216.
- Sagala FS, Harnack D, Bobrov E, Sohr R, Gertler C, James SD, Kupsch A (2012) Neurochemical characterization of the striatum and the nucleus accumbens in L-type Ca(v)1.3 channels knockout mice. *Neurochem Int* 60:229–232.
- Sapp E, Ge P, Aizawa H, Bird E, Penney J, Young AB, Vonsattel JP, DiFiglia M (1995) Evidence for a preferential loss of enkephalin immunoreactivity in the external globus pallidus in low grade Huntington's disease using high resolution image analysis. *Neurosci* 64:397–404.
- Shirendeb UP, Calkins MJ, Manczak M, Anekonda V, Dufour B, McBride JL, Mao P, Reddy PH (2012) Mutant huntingtin's interaction with mitochondrial protein Drp1 impairs mitochondrial biogenesis and causes defective axonal transport and synaptic degeneration in Huntington's disease. *Hum Mol Genet* 21:406–420.

- Stark H, Rothe T, Wagner T, Scheich H (2004) Learning a new behavioral strategy in the shuttle-box increases prefrontal dopamine. *Neurosci* 126:21–29.
- Surmeier DJ, Graves SM, Shen W (2014) Dopaminergic modulation of striatal networks in health and Parkinson's disease. *Curr Opin Neurobiol* 29:109–117.
- Tepper JM, Wilson CJ, Koos T (2008) Feedforward and feedback inhibition in neostriatal GABAergic spiny neurons. *Brain Res Rev* 58:272–281.
- Turrigiano GG (2008) The self-tuning neuron: synaptic scaling of excitatory synapses. *Cell* 135:422–435.
- von Nicolai C, Engler G, Sharott A, Engel AK, Moll CK, Siegel M (2014) Corticostriatal coordination through coherent phase-amplitude coupling. *J Neurosci* 34:5938–5948.
- Walker FO (2007) Huntington's disease. *Lancet* 369:218–228.
- Weihe E, Depboylu C, Schutz B, Schafer MK, Eiden LE (2006) Three types of tyrosine hydroxylase-positive CNS neurons distinguished by dopa decarboxylase and VMAT2 co-expression. *Cell Mol Neurobiol* 26:659–678.
- Wichmann T, DeLong MR, Guridi J, Obeso JA (2011) Milestones in research on the pathophysiology of Parkinson's disease. *Mov Disord* 26:1032–1041.

(Accepted 21 October 2015)
(Available online 4 November 2015)